

# InfoNEAT: Information Theory-based NeuroEvolution of Augmenting Topologies for Side-channel Analysis

Rabin Yu Acharya  
rabin.acharya@ufl.edu  
University of Florida  
Gainesville, FL, USA

Fatemeh Ganji  
fganji@wpi.edu  
Worcester Polytechnic Institute  
Worcester, MA, USA

Domenic Forte  
dforte@ece.ufl.edu  
University of Florida  
Gainesville, FL, USA

## ABSTRACT

Profiled side-channel analysis (SCA) leverages leakage from cryptographic implementations to extract the secret key. When combined with advanced methods in neural networks (NNs), profiled SCA can successfully attack even those crypto-cores assumed to be protected against SCA. Despite the rise in the number of studies devoted to NN-based SCA, existing methods could not systematically address the challenges involved in the NN-based SCA. A range of questions has remained unanswered, namely: how to choose a NN with an adequate size, how to tune the NN’s hyperparameters, when to stop the training, and how to explain the performance of the NN model in quantitative terms, in the context of SCA. Our proposed approach, “InfoNEAT,” tackles these issues in a natural way. InfoNEAT relies on the concept of evolution of NNs (both the network architecture and parameters, so-called neuroevolution), enhanced by information-theoretic metrics to guide the evolution, halt it with a novel stopping criteria, and improve time-complexity and memory footprint. The performance of InfoNEAT is evaluated by applying it to publicly available datasets composed of real side-channel measurements. In addition to the considerable advantages regarding the automated configuration of NNs, InfoNEAT demonstrates significant improvements over other approaches including a reduction in the number of epochs and width of the NN (i.e., the number of nodes in a layer) by factors of at least 1.25 and 6.66, respectively. According to our assessment and on the basis of our results, this is indeed achieved without any deterioration in the performance of SCA compared to the state-of-the-art NN-based methods.

## CCS CONCEPTS

• Security and privacy → Side-channel analysis and countermeasures; • Mathematics of computing → Information theory; • Computing methodologies → Ensemble methods; Neural networks;

## KEYWORDS

Side-channel Analysis; Neural Networks; Multi-layer Perceptrons; Evolutionary Strategies; Stacking; Information Theory

## 1 INTRODUCTION

Hardware security concerns secure key generation and storage as well as secure execution. While promising candidates have been proposed in the literature to deal with formers problems, the issue with secure execution continues to exist. Secure execution is a challenging goal to attain due to the leakage of information from implementations, often referred to as a side-channel. Attacks leveraging such leakages related to a secret key are strong in the sense

that various cryptographic algorithms have proven vulnerable to these attacks. The involvement of standardization and certification bodies in the activities related to the development of tools for leakage detection and side-channel analysis (SCA) further highlights the importance of this matter, see, e.g., [17, 46].

Prominent examples of side-channels include execution time, power consumption, and electromagnetic (EM) radiations collected from a target, e.g., a device embodying a cryptographic module such as an advanced encryption standard (AES) crypto-core. To analyze such side-channels, profiled attacks are common practice due to their effectiveness [5]. In the first phase of this attack (so-called profiling), the leakage from an open copy of the target device, is modeled under a controlled condition (e.g., known secret keys) cf. [14, 29, 35, 40]. Traditionally, such a model has been obtained by characterizing the leakages precisely through statistical techniques, e.g., linear regression [15, 56]. Afterward, in the second phase (so-called attack), this model is used to launch a key-recovery attack on the target device. These phases are in line with the specifics of machine learning (ML) tasks in the sense that the profiling and attack steps correspond respectively to the training and testing sub-tasks in the context of supervised ML. Interestingly enough, ML-enhanced SCA can defeat not only unprotected, see e.g., [27, 29, 36], but also protected cryptographic implementations [10, 21, 32, 35, 50, 65]. Furthermore, when only a limited number of traces with noise is available, ML-enhanced SCA approaches outperform the template attack [14], known to be optimal from an information-theoretic perspective if a large enough number of traces are available [6, 50]. The scenario, where only a few noisy traces are available, is of great importance as it reflects a more realistic scenario.

In this regard, it is not surprising that deep learning and NNs are now playing an active role in the SCA literature [26]. In particular, it has been demonstrated that NNs can further defeat some countermeasures designed to protect a cryptographic implementation. Specifically, the jitter-based misalignments in the side-channel traces, i.e., creating an array of asynchronous measurements, cannot stop an attacker from launching SCA through NNs [5, 9]. Even masked implementations, with countermeasures that randomize the intermediate values, can be successfully attacked by NNs [32, 50, 65]. Nevertheless, the state-of-the-art NN-based SCA requires further investigation to become more efficient and applicable in practice (see Section 2 for a detailed discussion). In this context, the design of NNs used for SCA needs to become less ad hoc by taking more systematic approaches into account. More concretely, these questions need to be answered, although they have remained open so far: *Which configurations and parameter combinations should be used? How can a trade-off between model complexity and training/testing errors be made? When can the training process be stopped?*

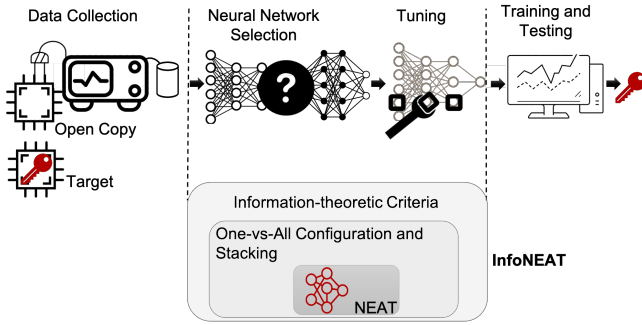


**Figure 1: Overview of the proposed “InfoNEAT” which extends the NEAT algorithm to meet SCA requirements. Compared to conventional ML-enabled SCA, network selection and parameter tuning are handled automatically.**

**InfoNEAT:** Our framework introduced in this paper, addresses these issues by building a novel algorithm that revolves around the notion of the evolution of NNs, so-called “neuroevolution.” The cornerstone of this concept is to evolve the *configuration of multiple networks (so-called augmenting topologies), and simultaneously tune their hyperparameters*. While the former ensures that a network suiting the purpose of the SCA is trained, the latter resolves one of the main problems that have remained open in the context of SCA. Specifically, it has been demonstrated that although NN-based attacks can extract the secret from even protected implementations, hyperparameter tuning imposes serious challenges to the application of NNs for SCA [32, 65, 69]. Interestingly, although neuroevolution can be employed in various domains, InfoNEAT is tailored to the specific requirements of SCA. The workflow of InfoNEAT is similar to common profiled attacks, see Figure 1. For existing NN-based attacks, in the training process, selecting the adequate configuration of the network and tuning the hyperparameters are typically based on trial and error. In fact, NN models that have been applied in the context of SCA are well studied in other domains, which might or might not share common characteristics with SCA. InfoNEAT, on the contrary, evolves various NNs and their hyperparameters and eventually delivers the one selected based on sound information-theoretic metrics. Regarding our **contributions** listed below and expounded upon in the paper, InfoNEAT is particularly powerful for SCA.

(1) **InfoNEAT tailors NEAT for SCA.** The original NEAT algorithm [60] cannot cope with complex multi-class classification tasks, specifically when many output neurons are involved. To cope with such task, InfoNEAT employs One-vs-All (sometimes called “One-vs-Rest”) multi-class classification followed by stacking ensemble learning. This is one of the novel aspects of InfoNEAT that conforms with the specification of SCA (see Section 5.3).

(2) **Estimation of intrinsic dimensionality (ID).** Traces collected from software and hardware implementations often contain thousands of features which leads to the well-known curse of dimensionality, i.e., SCA can become exponentially difficult in high dimensions. Nevertheless, similar to other ML tasks, this problem cannot be fully attributed to the number of features, but the intrinsic dimensionality (ID), i.e., the minimal number of parameters needed to describe a representation of a given dataset. For SCA,

we explore how the generalizability of compact NNs generated by InfoNEAT can be linked to the ID. Note that, to the best of our knowledge, our paper is the **first** to consider and report the ID of SCA traces.

(3) **Criteria for stopping the training/evolution processes in InfoNEAT.** It is evident that it is a time-consuming and memory-hungry process when evolving various NNs as done by the original NEAT algorithm. To address this, InfoNEAT is equipped with mechanisms relying on Information theory. Intuitively, the information-theoretic conditions indicate whether adding a new connection/node can help improve InfoNEAT’s output. If not, the evolution process is stopped. Moreover, the proposed criteria is useful to guides the evolution process when it comes to selecting the best NN among ones evolved by InfoNEAT.

(4) **Key-recovery attacks using InfoNEAT.** Last but not least, we evaluate the effectiveness of InfoNEAT against a state-of-the-art side-channel trace database and ML models that have become the standard benchmarking system for SCA. According to our results, InfoNEAT enhances the memory and time efficiency of SCA by reducing the number of nodes in hidden layers and the training epochs<sup>1</sup> by factors of 6.6 and 1.25, respectively. This is achieved without resulting in over- or under-fitting or impairing the key recovery performance compared to relevant NN-based attacks.

We stress that our results provide proof of concept of how InfoNEAT is helpful in the field of SCA. Nonetheless, we believe that InfoNEAT can have the potential to be adapted and become one of the powerful tools for security-related problems.

**Outline:** The rest of the paper is organized as follows. Section 2 gives a brief overview of the most relevant studies in the literature. In Section 3, profiled SCA along with our notations and mathematical principles are discussed. Afterward, in Section 4, we introduce the NEAT algorithm as a building block of our proposed algorithm InfoNEAT described in Section 5. To support why InfoNEAT fits the purpose of SCA, Section 6 discusses how to compute the ID of a dataset and its implications for SCA. This is then followed by Section 7, where the results of our experiments are presented and discussed. Finally, Section 8 concludes the paper.

## 2 RELATED WORK

Machine learning techniques have become quite popular and successful in profiled SCA in recent years. Among them, multilayer perceptron (MLP) and convolutional neural networks (CNNs) are the two most widely used [26, 52, 63, 64]. However, these works rely on massive networks (which usually lead to *overfitting*), have complex and unclear design methodologies, tune the network hyperparameters in a *trial-and-error* based manner (i.e., not automatically), and rely on models that are often not *generalizable*. All of these issues and shortcomings can be addressed with our InfoNEAT framework. In this section, we explain these issues as well as the related state-of-the-art works in more detail. A summary of the related works as well as the comparison with InfoNEAT are also included in Table 4 (see Appendix A).

<sup>1</sup>The number of epochs is the number of times a learning algorithm sees the entire training dataset.

## 2.1 Use of MLP Networks vs. CNNs

In [26, 28], the authors mention that CNNs could outperform other NN-based attack techniques because of their effectiveness with raw data, especially in the presence of jitter or desynchronization. This comparison, however, is irrelevant in the field of SCA as most of the techniques have traditionally only considered ML metrics to evaluate their models [50, 52]. In this regard, the authors in [50] show that when considering SCA-related metrics, both models (CNN and MLP) perform similarly well, especially when combined with SMOTE (Synthetic Minority Oversampling Technique). Picek et al. in [52] showed that MLPs equipped with XGBoost outperform CNN when considering pure SCA metrics such as the guessing entropy. Furthermore, they suggest that the slight performance boost offered by CNN may not be worthwhile due to how complex, time-consuming, and resource-intensive it is to design. Nevertheless, they develop large MLP networks which are only tested on the same dataset as training rather than different variants of the dataset or a new dataset (see Section 7.5 for our results in the former case). This leads us to the one of the major issues in SCA community, *Generalization*.

## 2.2 The Issue of Generalization

Generalization is the ability of a SCA model trained on one dataset to adapt well to new, unseen data. In this regard, the authors in [62] demonstrate attacks on different SCA datasets and show how MLPs are internally the same despite changing the device or the key because MLPs are considered universal approximators. Furthermore, even small MLP networks were shown to roughly learn the same function without overfitting and generalize to different datasets [51, 62]. Generalization has also been addressed in [49], where the authors show how ensembles of models based on averaged class probabilities can further improve the network generalization to various datasets. The model selection performed in the context of InfoNEAT is similar to the “bucket of models” ensemble method presented in [49]. This is indeed helpful to improve the generalization for each class (i.e., each guessed sub-key). Furthermore, both InfoNEAT and the approach in [49] turn towards small as well as an ensemble of models to improve the generalization. Indeed, the generalizability of InfoNEAT is further boosted by employing stacking learning to improve the generalization among various classes. However, in contrast to InfoNEAT, the models in [49, 51, 62] are designed on a trial-and-error basis. The tuning of the network (*hyperparameters*) is not even considered in most of the studies, and when they are considered, the process is not automated to reach peak SCA performance like InfoNEAT.

## 2.3 Semi-automated Hyperparameter Tuning

This leads us to a few recent works which consider tuning of hyperparameters – the number of nodes, number of layers, and number of epochs – and even fewer that try to automate this process [48, 54, 65]. In [48], the authors suggest tuning hyperparameters while trying to prevent underfitting or overfitting by defining stopping criteria rather than a pre-defined number of epochs or by relying solely on SCA metrics and trial-and-error. Although InfoNEAT shares a similarity with [48], namely relying on an information-theoretic measure to stop the training, we neither train

NNs by minimizing the IB function [2], nor consider the so-called fitting and compression phases [55]; hence, the issues inherent to these methods [55] are avoided by InfoNEAT (see Section 5.2).

In recent years, several automated methods to tune the hyperparameters have also been proposed. [54] uses Reinforcement Learning (RL) while [65] uses Bayesian optimization. The work in [54] is automatic but only applicable to CNNs. [65] explores different MLP network architectures by trial-and-error and uses optimization algorithms, such as Bayesian optimization and Random Forest, to optimize the weights of the architecture. InfoNEAT, on the other hand, tunes the size, structure, and weights of the network. It starts from a very small network and, with the aid of evolutionary techniques and information-theoretic analysis, increases the size of the architecture and changes the weights of the network.

## 3 BACKGROUND AND MATHEMATICAL FOUNDATIONS

### 3.1 Notations

In this paper, the calligraphic letters, e.g.,  $\mathcal{X}$ , are used to denote sets. Moreover, bold letters (e.g.,  $\mathbf{y}$ ) correspond to matrices and vectors. We use the standard notations for mathematical operators defined in the respective sections. For a random variable  $X$ , the corresponding lower-case letter  $x$  denotes realizations of  $X$ . In addition, we refer to NNs as models or sub-models, networks, and genomes.

### 3.2 Profiled Side-channel Analysis

One of the most powerful forms of side-channel attack is the profiled SCA in which the adversary uses a device that he can control to build a *profiling model* that can then later be used to extract the encryption key from similar devices. After the introduction of profiling attacks in [14], due to their close conceptual connection with ML tasks, ML-based attacks were proposed to enhance them. Thus, the profiled SCA has two steps: a *profiling* (similar to training in the context of ML) step and an *attack* (or testing as known in ML domain) step. During the first step (profiling), the adversary has access to a test device and can control its (guessable or public) inputs, which are a chunk of plaintext  $P$ , as well as a part of the cryptographic algorithm’s secret key  $S$  that the attacker aims to disclose. The observations made by feeding these inputs can be seen as an estimation  $\hat{\varphi}_s$  of the conditional probability distribution function for every possible  $s \in \mathcal{S}$  as defined below cf. [5].

$$\varphi_s : (\mathbf{x}, s) \mapsto \Pr[\mathbf{X} = \mathbf{x} \mid (P, S) = (p, s)].$$

In other words, the traces collected by the attacker can be used to come up with the estimation  $\hat{\varphi}_s$ . Precisely, for a given set of  $\{p_i, s_i\}_{i=1}^n$ , the attacker collect  $n$  traces  $\{x_1^i, x_2^i, \dots, x_k^i\}_{i=1}^n$ , where each trace contains  $k$  features ( $k \geq 2$ ). Based on this “profiling data set”, the adversary constructs a machine learning model (i.e., a leakage model) that can estimate the probability of inputs for each trace:  $\hat{\varphi}_{X,P} : (\mathbf{x}, p) \mapsto \Pr[(P, S) = (p, s) \mid \mathbf{X} = \mathbf{x}]$  for every  $s \in \mathcal{S}$ .

During the second step (attack), the attacker attempts to classify a set of  $N_{test}$  traces, the so-called test set corresponding to an unknown  $s$ , based on the above leakage model. Formally, the attacker should derive the label for a trace, similar to a ML classification problem:  $\mathbf{y} = \hat{\varphi}_{X,P}(\mathbf{x}, p)$ , for  $\hat{s} \in \mathcal{S}$  so that  $\hat{s} = \arg \max_{s \in \mathcal{S}} \mathbf{y}_k$ , where  $\mathbf{y}_k$  is the  $k^{\text{th}}$  entry in the vector  $\mathbf{y}$ . For  $N_{test}$  traces, a *score*

based on the maximum-likelihood of each hypothetical key can be obtained as  $\mathbf{d}_k = \prod_{i=1}^{N_{test}} \mathbf{y}_k^i$ , where  $\mathbf{y}_k^i$  is the  $k^{\text{th}}$  entry in the vector  $\mathbf{y}^i$  corresponding to the  $i^{\text{th}}$  trace. Based on this score, the key hypotheses are ranked in a decreasing order based on the rank function (Equation (1)), from which the attacker chooses the key that is ranked first. The rank function is defined as follows cf. [5].

$$\text{Rank}(\hat{\varphi}, N_{test}) = |\{k \mid \mathbf{d}_k > \mathbf{d}_{k^*}\}|, \quad (1)$$

where  $k^*$  represents the key that has been used during the acquisition of the profiling traces. Note that the rank is computed for a collection of  $N_{test}$  traces from the test dataset, where  $N_{test}$  is increased gradually until the rank is minimized (lower the rank, higher the score). Since the rank is dependent on the traces used, it is common practice to compute the rank over different folds of datasets and compute an *average rank*, also called the *guessing entropy*. On a side-note, when reviewing the relevant literature, to test the ML model trained during the profiling process, one observes that either the guessing entropy or the rank function is used as a metric for SCA effectiveness. However, both are exactly the same as described in [39]. Thus, we use the term ‘‘average rank’’ throughout this paper to refer to the rank function or the guessing entropy.

**3.2.1 ASCAD Dataset.** ASCAD is a dataset introduced in [5] which consists of electromagnetic (EM) radiations emitted from the software implementation of AES-128 protected with first-order Boolean masking and running on an 8-bit AVR microcontroller ATmega8515. This dataset is structured similar to a typical ML dataset and consists of 50,000 training (or profiling) traces and 10,000 testing (or attack) traces. Each trace contains 700 sample points which represent the measurements for various intermediate values related to the processing of the third S-box. In addition, the dataset also contains the *labeled data*, which represents the output of the third S-box during the first round as labels for each trace, leading to 256 classes. This is due to the fact that SCA often concerns recovering key bytes (i.e., sub-keys) to not only simplify the process, but also reflect how the key is usually fed into a cryptographic implementation [29, 59]. In this way, one key byte is considered as an example of all 16 bytes in a 128-bit AES [71]. Thus, there are 256 classes in the classification problem for the key byte recovery.

Among datasets offered in the ASCAD framework, we consider the following ones collected from a device operated with a fixed key. ASCAD also offers traces with random keys which will be a focus of our future work.

- The dataset which contains synchronized traces with no jitter which we will refer to as **ASCADsync**.
- The dataset which contains desynchronized traces with a 50 samples window maximum jitter which we will refer to as **ASCADdesync50**.
- The dataset which contains desynchronized traces with a 100 samples window maximum jitter which we will refer to as **ASCADdesync100**.

### 3.3 Mathematical Principles

**3.3.1 Matrix-based Rényi Entropy.** One of the recent and major breakthroughs in information theory is the new estimator of Rényi entropy in a matrix form as defined below. In particular, using this estimator, it has become feasible to understand the information flow

without knowing the probability density functions [67, 68]. This estimator is the basis of the NN selection and algorithm stopping criteria introduced in InfoNEAT.

**DEFINITION 1.** (cf. [67]) *Given a set of  $n$  samples  $\{x_1^i, x_2^i, \dots, x_k^i\}_{i=1}^n$ , where each sample contains  $k$  ( $k \geq 2$ ), we define the kernels  $\kappa_1 : X_1 \times X_1 \mapsto \mathbb{R}, \dots, \kappa_k : X_k \times X_k \mapsto \mathbb{R}$  ( $X_z = x_z^1, \dots, x_z^n$  with  $1 \leq z \leq k$ ), which are real-valued positive definite and infinitely divisible [7, 67]. The Rényi’s  $\alpha$ -order joint-entropy among  $k$  variables is*

$$J_\alpha(\mathbf{X}_1, \dots, \mathbf{X}_k) = S_\alpha \left( \frac{\mathbf{A}_1 \odot \dots \odot \mathbf{A}_k}{\text{tr}(\mathbf{A}_1 \odot \dots \odot \mathbf{A}_k)} \right), \quad (2)$$

where  $(\mathbf{A}_1)_{ij} = \kappa_1(x_1^i, x_1^j), \dots, (\mathbf{A}_k)_{ij} = \kappa_k(x_k^i, x_k^j)$ .  $\text{tr}(\cdot)$  and  $\odot$  denote the transpose and Hadamard product operators, respectively. Furthermore, the function  $S_\alpha(\cdot)$  is defined as follows.

$$S_\alpha(\mathbf{A}) = \frac{1}{1-\alpha} \log_2(\text{tr}(\mathbf{A}^\alpha)) = \frac{1}{1-\alpha} \log_2 \sum_{i=1}^n \lambda_i(\mathbf{A}^\alpha), \quad (3)$$

where  $\lambda_i(\mathbf{A})$  denotes the  $i^{\text{th}}$  eigenvalue of  $\mathbf{A}$ .

There is a relationship between the matrix  $\mathbf{A}$  as defined in Equation (3) and the Gram matrix  $\mathbf{K}$ . In this regard,  $\mathbf{A}_{ij} = \frac{\mathbf{K}_{ij}}{n\sqrt{\mathbf{K}_{ii}\mathbf{K}_{jj}}}$ .

**3.3.2 Intrinsic Dimension (ID) Estimation.** This section gives an overview of concepts needed to estimate the ID of a dataset, i.e., the minimal number of parameters needed to describe it (for an extensive survey on ID estimation, see [11]). Formally, for a given dataset  $X = \{x_1^i, x_2^i, \dots, x_k^i\}_{i=1}^n \subset \mathbb{R}^D$ , the feature vectors  $\mathbf{x}^i$  ( $1 \leq i \leq n$ ) are seen as points constrained to lie on a low dimensional manifold with the intrinsic dimension  $d$  so that  $\mathcal{M} \subseteq \mathbb{R}^d$ , embedded in a higher dimensional space  $\mathbb{R}^D$  cf. [13]. In other words, the ID of  $X$  is equal to  $d$  if its elements lie within a  $d$ -dimensional subspace of  $\mathbb{R}^D$ . To estimate the ID, one of the most acknowledged methods is principal component analysis (PCA) *projecting* the input  $X$  on the  $d$  directions of maximum variance [33]. Despite its popularity, PCA and, in general, projection-based methods cannot offer reliable ID due to their sensitivity to noise and parameter settings [37]. To cope with this, geometric algorithms have been proposed that can be categorized based on statistics used to estimate the ID. The statistics correspond to either the distances between neighboring points or the fractal dimension, where the statistics are functions of the ID.

Among various geometric techniques to perform the ID estimation, in this paper, we discuss and compare the results of three algorithms as follows.

**Correlation Dimension (CorrDim):** This fractal dimension-based estimate of  $d$  relies on the assumption that every point in  $X$  is drawn uniformly from  $\mathbb{R}^d$ . The CorrDim, and consequently  $d$ , is estimated following the principle of the correlation integral  $C(r)$  calculated as  $C(r) = \lim_{k \rightarrow +\infty} g/k^2$ , where  $g$  is the total number of pairs of points with distance less than  $r$ . The correlation integral scales as  $C(r) \sim r^d$  when  $r \rightarrow 0$ ; hence, the ID  $d$  can be measured as the slope of the correlation integral as a function of  $r$  in log-log scale  $d = \lim_{r \rightarrow 0} \log(C(r))/\log r$ , cf. [16].

**DANCo:** CorrDim is an effective estimator of small IDs ( $d \leq 10$ ); however, it systematically underestimates the ID of manifolds with

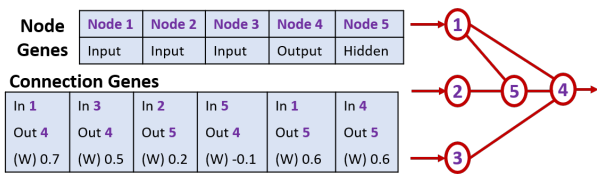


Figure 2: A typical genome or network created in NEAT. ( $W$ ) denotes the weight assigned to each connection.

larger IDs [16]. In order to resolve this issue, a generalization of CorrDim based on  $k$ -nearest-neighbors distances is proposed [13]. Their algorithm, so-called DANCo, exploits the normalized nearest neighbor distances and the angles computed on couples of neighboring points. Precisely, DANCo estimates the ID by exploiting the theoretical joint distribution between the norms and angles of the points, denoted by  $h_d(r, \theta)$ . Similarly, an empirical joint distribution  $\hat{h}_d(r, \theta)$  is derived from the dataset  $X$ . The ID then can be estimated as follows.

$$d = \arg \min_{1 \leq d \leq D} \int_{-\pi}^{\pi} \int_0^1 h_d(r, \theta) \log \left( \frac{h_d(r, \theta)}{\hat{h}_d(r, \theta)} \right) dr d\theta$$

Obviously, it is not straightforward to derive the theoretical  $h_d(r, \theta)$  and estimate  $\hat{h}_d(r, \theta)$ . Nevertheless, the above estimation can be performed by applying two Kullback-Leibler divergences applied to the distribution of normalized nearest-neighbor distances and the distribution of pairwise angles of the points cf. [13]. The implementation of this algorithm is provided by the authors in [38].

**Full Correlation Integral (FCI):** This estimator recently proposed by [16] is one of the most powerful techniques presented in the literature so far. Its ultimate goal is to overcome the shortcomings of the algorithms mentioned above by proposing a technique that is robust to non-uniform sampling (e.g., under-sampling of datasets with a large ID) and the noise. In fact, their proposed methods relying on the notion of full correlation integral can be seen as an extension of the CorrDim estimator. Specifically, FCI does not impose any limit on the distance between the points, in contrast to CorrDim. In this regard, for the manifold,  $\mathcal{M}$ , FCI is defined as the average correlation integral over a range of distances.

## 4 NEUROEVOLUTION OF AUGMENTING TOPOLOGIES (NEAT)

For the sake of completeness, this section gives a brief overview of how the neuroevolution of augmenting topologies (NEAT) algorithm works as needed to understand InfoNEAT. For more details, the reader is referred to [60]. The fundamental process taking place in NEAT is similar to the evolution of organism’s genomes, where genomes represent NNs, see Figure 2. In particular, the main idea behind NEAT is the concept of neuroevolution, which searches for network topologies by means of evolutionary algorithms (EAs). In doing so, the EA optimizes hyperparameters of deep networks, specifically, the weights of individual neurons and their inter-connections are evolved in each step, called a *generation*, see Figure 3(a).

Although NEAT variants can be comprised of various types of NNs, e.g., convolutional NNs, we stick to a variant evolving MLP-like NNs in this paper. NNs are grouped in species based on their randomly chosen structures. In each generation, several species

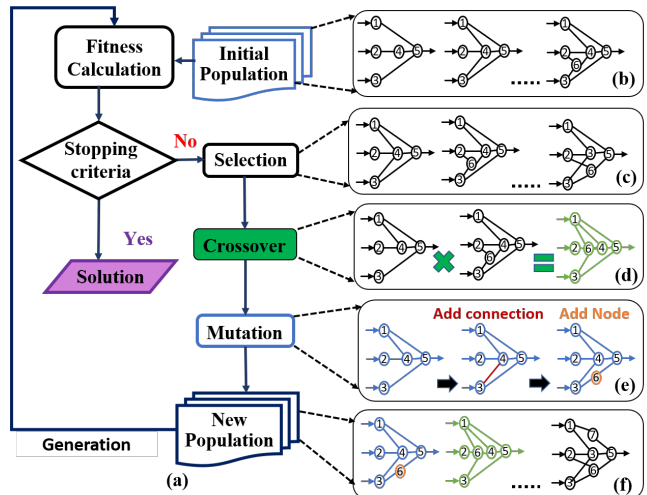


Figure 3: A general overview of the evolution mechanism involved in NEAT, and consequently, InfoNEAT.

---

### Algorithm 1: NEAT Algorithm cf. [20]

---

- Input:** Batch size data of input dataset  $D$ ; Population size  $N$ ; Initial number of hidden nodes  $n_h$ ; Fitness threshold  $f_t$ ; Connection add probability  $P_c$ ; Node add probability  $P_n$ ; Number of generations  $T$ ; Compatibility threshold  $t_c$ ; Weights and bias mutation rate  $P_w$  and  $P_b$ , respectively;
- 1 **Initialization:** Generate a set of genomes or networks  $g_{t=1,i}$  ( $1 \leq i \leq N$ ) randomly based on  $N$  and  $n_h$ ;
  - 2 **for**  $t = 1, 2, \dots, T$  **do**
  - 3     **Fitness evaluation:** Compute the fitness (e.g., cross-entropy loss) for  $g_{t,i}$ ;
  - 4     **if** fitness values  $L_{t,i} \leq L_{TH}$  **then break; else continue; end**
  - 5     **Selection:** Select the best individuals and producing a new generation  $g_{t+1,i}$  with a Russian roulette process on  $g_{t,i}$ ;
  - 6     **Crossover:** Individuals with genomic distance  $< t_c$  are part of the same species and are selected for crossover;
  - 7     **Mutation:** For each individual  $g_{t,i}$ , the mutation of weights and bias is performed based on  $P_w$  and  $P_b$  respectively and the structural mutation is performed based on  $P_c$  and  $P_n$ ;
  - 8 **end**
- 

(i.e., sub-populations) exist that share a similar topology (i.e., the way that the nodes are connected to each other). In this regard, the genomes in different species can have different sizes. Independent from other species, each species evolves proportionally to its fitness so that the weights of NNs are learned. Learning the weights of NNs has conventionally been performed without backpropagation.

Figure 3 illustrates the main steps involved in NEAT (see Algorithm 1) as explained below.

**Initial population (line #1 in Algorithm 1):** The population considered by NEAT contains NNs, i.e., the genomes (see Figure 2) that are denoted by  $g_{t,i}^j$ , where superscript  $j$  ( $1 \leq j \leq \ell$ ) indicates the  $j^{\text{th}}$  layer. Moreover, the subscripts  $t$  and  $i$  denote the generation and the  $i^{\text{th}}$  NN in the species, respectively. In the first generation  $t = 1$ , the total number of NNs in all species is  $N$  and each species contains  $N_{s,t=1}$  NNs. For the sake of simplicity and without loss of generality, we explain the learning/evolution phase for one species. Features at the input of each genome and the output class labels

are denoted by  $\mathbf{X}$  and  $\mathbf{Y}$ , respectively. The evolution process begins with a set of NNs with minimal complexity. In the first generation, in a species, each NN  $g_{1,i}^1$  ( $1 \leq i \leq N_{s,1}$ ) is composed of  $j = 1$  hidden layer. The output of each layer is a function of the input  $\mathbf{X}$ , the matrix of weights between  $j^{\text{th}}$  and  $(j + 1)^{\text{th}}$  layers  $\mathbf{W}_j$  and the vector of biases for the  $(j + 1)^{\text{th}}$  layer  $\mathbf{b}_{j+1}$  ( $1 \leq j \leq \ell$ ). More specifically, for a set of weights and biases  $\theta_j = \{\mathbf{W}_j, \mathbf{b}_{j+1}\}$ , the function  $f : \mathbb{R}^{|\theta_j|} \rightarrow \mathbb{R}^{|\theta_{j+1}|}$  is applied to the weights, biases and inputs to generate the output at the  $(j + 1)^{\text{th}}$  as follows:  $\hat{\mathbf{y}}_{j+1} = f(\hat{\mathbf{y}}_j \mathbf{W}_j + \mathbf{b}_{j+1})$ , where  $\hat{\mathbf{y}}$  and  $f(\cdot)$  denote the estimated label and the activation function, respectively.

**Fitness evaluation and selection (lines #3–5 in Algorithm 1):** One of the differences between the NNs usually applied in various domains and NEAT as a neuroevolutionary algorithm is that all the NNs in a species are evaluated based on a fitness function. According to this probabilistic evaluation, the algorithm decides which NNs would be successful in the next generations. This is accomplished by assigning a fitness value to each genome. Afterward, the fitness values are taken into account by a selection operator, e.g., tournament selection [20] (see Figure 3(c)).

**Crossover (lines #6 in Algorithm 1):** The steps corresponding to fitness evaluation and selection are then followed by the crossover operation, also known as recombination, where the genetic information (e.g., the parameters of the NNs) of two selected individuals are combined as shown in Figure 3(d).

**Mutation (lines #7 in Algorithm 1):** For each non-crossover individual, random changes are made into the NNs based on the mutation operator, as shown in Figure 3(e). Specifically, nodes and connections are added incrementally to these NNs in each generation to update configurations and parameters.

The steps above are repeated until a condition is met, e.g., typically when a maximum number of generations are executed.

## 5 INFONEAT

This section gives details on InfoNEAT, which is built upon NEAT. Variants of the NEAT algorithm have been developed accordingly, which are used for various tasks, including regression [24], classification [24, 60], and reinforcement learning (RL) [57]. Nevertheless, in this paper, we stick to NEAT’s application to classification. First, we explain which fitness function can be applied to tailor NEAT for SCA. It is followed by how the information-theoretic stopping criteria are defined for InfoNEAT. Finally, we discuss the challenges that were faced when designing and implementing InfoNEAT.

### 5.1 Adequate Fitness Function for SCA

The fitness function evaluating the performance of the NNs in each generation helps to select the NNs that will be evolved in the next generations. For a given genome (e.g.,  $i^{\text{th}}$  NN) in the  $t^{\text{th}}$  generation, InfoNEAT employs the categorical cross-entropy loss function to compute the loss  $L_{t,i}$  formulated as

$$L_{t,i} = - \sum_{k=1}^{|\mathbf{y}_{t,i}^\ell|} y_k \log \hat{y}_k,$$

where  $y_k$  and  $\hat{y}_k$  are the  $k^{\text{th}}$  entries in  $\mathbf{y}_{t,i}^\ell$  and  $\hat{\mathbf{y}}_{t,i}^\ell$ , respectively. When it comes to computing the cross-entropy for classification

---

### Algorithm 2: Genome selection based on fitness and CMI

---

**Input:** Number of genomes within a species  $N_s$ ; All the genomes in a species  $g_{t,i}^j$  ( $1 \leq i \leq N_s$  and  $1 \leq j \leq \ell$ );

**Result:** Best genome within a species  $g_{t,s}^j$ ;

- 1 **Initialization:** Calculate the loss values  $L_{t,i}$  for  $1 \leq i \leq N_{s,t}$ ;
- 2 **if** number of genomes with  $\min_{1 \leq i \leq N_s} (L_{t,i})$  is one **then**
- 3     break;
- 4 **else**
- 5      $G = \{g_{t,i}^j \mid L_{t,i} = \min_{1 \leq i \leq N_{s,t}} (L_{t,i})\}$ ;
- 6     **for**  $g_{t,i}^j \in G$  **do**
- 7         **for**  $j = \ell, \ell - 1, \dots, 1$  **do**
- 8              $\text{CMI} = \mathbf{I}(\hat{\mathbf{y}}_{t+1,i+1}^j; \mathbf{y} \mid \hat{\mathbf{y}}_{t,i+1}^j)$ ;
- 9             **if** number of genomes with  $\min_{1 \leq i \leq N_{s,t}} (\text{CMI})$  is one **then**
- 10                 break;
- 11             **else**
- 12                 continue;
- 13             **end**
- 14         **end**
- 15     **end**
- 16 **end**

---

tasks, the terms “cross-entropy” and “negative log-likelihood” are used interchangeably [44]. This is of great importance to SCA as it has been proven that negative log-likelihood (NLL) is inversely related to “perceived information” [8, 41, 53]. The latter refers to the generalization of the mutual information between the side-channel traces and the leakage profiling model (i.e., the ML trained on the traces). In other words, the perceived information quantifies how well the ML model is trained. More interestingly, minimizing the NLL loss function (similarly, cross-entropy) during NN training is asymptotically equivalent to maximizing the perceived information and improving the trained NN performance cf. [41].

### 5.2 Information Theoretic Criteria

Conventionally, a maximum number of generations is defined, usually accompanied by another stopping criterion relying on the heuristic, e.g., if the accuracy of the best NN (i.e., the NN with the highest accuracy) does not improve after some generations, halt the evolution. To address this, InfoNEAT applies information theory-based approaches to select the genomes (NNs) to be evolved (see the part highlighted in blue in Algorithm 1) as well as to stop the evolution process. We stress that our methods are different from the proposals falling within the scope of information bottleneck (IB) [48]; hence, we neither train NNs by minimizing the IB function [2], nor consider the so-called fitting and compression phases [55]. InfoNEAT is inspired by and based mainly upon the study presented in [67].

In our approach, each mutated NN is seen as a randomly permuted one. Intuitively, making any change in a NN (i.e., evolving the NN in the next generation) should result in a monotonic decrease in the conditional mutual information (CMI) that is  $\mathbf{I}(\hat{\mathbf{y}}_{t+1,i}^j; \mathbf{y} \mid \hat{\mathbf{y}}_{t,i}^j)$ , where  $\hat{\mathbf{y}}_{t,i}^j$  denotes the output of a given layer in  $g_{t,i}^j$ . This is according to permutation tests [23] and well-described in [19] as an impact of adding useless variables (i.e., parameters associated with evolved NN). Below, we formalize this more precisely.

**5.2.1 Selection of the Best Genomes:** As discussed before, from each species, a set of NNs are evolved in the next generation. The



evolution of NNs from one generation to the next is considered as a permutation (without permuting the corresponding  $\mathbf{y}$ ). This is conceptually similar to what has been discussed for feature selection [19, 67] and determining the number of filters in convolutional NNs [68]. Nevertheless, in those studies, the permuted NNs have not been generated automatically as opposed to our approach.

To choose one or more NNs from a species, InfoNEAT discards NNs (e.g.,  $(i + 1)$ <sup>th</sup> genome), when the CMI  $\mathbf{I}(\hat{\mathbf{y}}_{t+1,i+1}^j; \mathbf{y} | \hat{\mathbf{y}}_{t,i}^j)$  is not significantly smaller than  $\mathbf{I}(\hat{\mathbf{y}}_{t+1,i}^j; \mathbf{y} | \hat{\mathbf{y}}_{t,i}^j)$  (see lines #6–15 in Algorithm 2). This means that if the mutated NNs cannot outperform the respective ones in the previous generation, those NNs are discarded. For this purpose, we combine this CMI-based criterion with the selection criterion offered in NEAT, which is based on the loss function as explained in Algorithm 2, line #2. Next, we elaborate on how the CMI is *estimated* for InfoNEAT.

### CMI computation based on Matrix-based Rényi's $\alpha$ -entropy:

This notion encompasses the extension of Shannon's entropy; however, in its traditional form, the probability distribution function (PDF) should be accurately estimated. To cope with this, we follow the procedure presented in [22, 66] that relies on the principle of the Gram matrix obtained from evaluations of a positive definite kernel from data samples, see Definition 1. This allows a direct estimation of the entropy and joint entropy between two or multiple variables from data without PDF estimation. The multivariate matrix-based Rényi's  $\alpha$ -entropy can be applied to estimate the CMI in high-dimensional space as follows cf. [67] (see Equation (2)).

Suppose that  $|\hat{\mathbf{y}}_{t+1,i}^j| = k_{t+1}$  and  $|\hat{\mathbf{y}}_{t,i}^j| = k_t$  denoting the number of outputs at the  $j$ <sup>th</sup> layer of the  $i$ <sup>th</sup> genome in the generations  $t + 1$  and  $t$ , respectively. Then,

$$\begin{aligned} & \mathbf{I}_\alpha(\{\mathbf{C}_1, \mathbf{C}_2, \dots, \mathbf{C}_{k_{t+1}}; \mathbf{B}\} | \{\mathbf{A}_1, \mathbf{A}_2, \dots, \mathbf{A}_{k_t}\}) = \\ & = \mathbf{S}_\alpha \left( \frac{\mathbf{A}_1 \odot \dots \odot \mathbf{A}_{k_t} \odot \mathbf{C}_1 \odot \dots \odot \mathbf{C}_{k_{t+1}}}{\text{tr}(\mathbf{A}_1 \odot \dots \odot \mathbf{A}_{k_t} \odot \mathbf{C}_1 \odot \dots \odot \mathbf{C}_{k_{t+1}})} \right) + \\ & + \mathbf{S}_\alpha \left( \frac{\mathbf{A}_1 \odot \dots \odot \mathbf{A}_{k_t} \odot \mathbf{B}}{\text{tr}(\mathbf{A}_1 \odot \dots \odot \mathbf{A}_{k_t} \odot \mathbf{B})} \right) - \mathbf{S}_\alpha \left( \frac{\mathbf{A}_1 \odot \dots \odot \mathbf{A}_{k_t}}{\text{tr}(\mathbf{A}_1 \odot \dots \odot \mathbf{A}_{k_t})} \right) - \\ & - \mathbf{S}_\alpha \left( \frac{\mathbf{A}_1 \odot \dots \odot \mathbf{A}_{k_t} \odot \mathbf{B} \odot \mathbf{C}_1 \odot \dots \odot \mathbf{C}_{k_{t+1}}}{\text{tr}(\mathbf{A}_1 \odot \dots \odot \mathbf{A}_{k_t} \odot \mathbf{B} \odot \mathbf{C}_1 \odot \dots \odot \mathbf{C}_{k_{t+1}})} \right). \quad (4) \end{aligned}$$

In Equation (4),  $\mathbf{A}_1, \dots, \mathbf{A}_{k_t}, \mathbf{B}, \mathbf{C}_1, \dots, \mathbf{C}_{k_{t+1}}$  denote the Gram matrices evaluated over  $\hat{\mathbf{y}}_{t,i}^j, \mathbf{y}$ , and  $\hat{\mathbf{y}}_{t+1,i}^j$ , respectively. Moreover,  $\mathbf{S}_\alpha(\cdot)$  and  $\odot$  denote the Rényi's  $\alpha$ -entropy and the Hadamard product (see Definition 1). This equation is the core of Algorithm 2 (line #8) for how InfoNEAT selects the genomes to be evolved. Note that this algorithm is run in every generation when the genomes' parameters are updated.

As can be seen in Algorithm 2, the CMI is computed to compare the genomes in two consecutive generations in a layer-wise manner. Interestingly, this comparison is first applied to the last layers of the genomes in the sense that if the CMI values are the same for the last layers of the genomes  $j = \ell$ , the second to last layer  $j = \ell - 1$  is considered and so on. This is due to the fact that the layer-wise mutual information between the labels and the outputs of a layer is minimized at the last hidden layer. This value increases so that its maximum can be observed at the first hidden layer [55, 58, 70]. Therefore, our layer-wise comparison implies

---

### Algorithm 3: Stopping criteria based on fitness and CMI

---

**Input:** Best genomes in the current generation  $g_{t,*}^\ell$  and in the generation  $g_{t-1,*}^\ell$  (i.e., the output of Algorithm 2); Genomes evolved from  $g_{t,*}^\ell$  in the next generation  $g_{t+1,i}^\ell$  ( $1 \leq i \leq N_{s,t+1}$ );

**Result:** Stop the training or evolution process and deliver the best genome  $g_{T,*}^\ell$  ( $T \geq 2$ );

```

1 Initialization: Calculate the loss  $L_{t+1,i}$  for  $g_{t+1,i}^\ell$  as well as  $L_{t,*}$ , i.e., the loss for the best genome  $g_{t,*}^\ell$ ;
2  $\text{CMI}_t = \mathbf{I}(\hat{\mathbf{y}}_{t,*}^\ell; \mathbf{y} | \hat{\mathbf{y}}_{t-1,*}^\ell)$ ;
3 for  $i = 1, \dots, N_{s,t+1}$  do
4   if  $L_{t,*} < L_{t+1,i}$  then
5     break and  $g_{T,*}^\ell = g_{t,*}^\ell$ ;
6   else
7      $\text{CMI}_{t+1} = \mathbf{I}(\hat{\mathbf{y}}_{t+1,i}^\ell; \mathbf{y} | \hat{\mathbf{y}}_{t,i}^\ell)$ ;
8     if  $\text{CMI}_t < \text{CMI}_{t+1}$  then
9       break and  $g_{T,*}^\ell = g_{t,*}^\ell$ ;
10    else continue;
11  end
12 end
13 end
14 end

```

---

that for the best genome selected through Algorithm 2, the mutual information between the labels and the outputs of the last layer can stay minimized [18].

**5.2.2 Stopping Criteria:** Our method to deal with the definition of a stopping criterion relies on the notions discussed for selecting the best genome from a species. In fact, the stopping mechanism can be seen as a continuation of the process associated with best genome selection. Compared to one of the most relevant approaches presented in [67], no threshold is needed to stop the algorithm. In the same vein as discussed in [68], InfoNEAT makes a decision based on the change in the CMI value, following the so-called CMI-permutation concept [67]. In contrast to [68], the permuted NNs are evolved by InfoNEAT automatically and randomly evolved from one generation to the next. To halt the process, we monitor not only the CMI values, but also the fitness values that are the cross-entropy loss (see Section 4).

Algorithm 3 explains this further. In the initialization phase (line #1), the loss function for the genomes in the current generation  $t + 1$  and the best genome  $g_{t-1,*}^\ell$  delivered by the Algorithm 2 is computed. An interesting observation is that to define the stopping criteria, similar to Algorithm 2, the last layers of the genomes are taken into account. This is due to the fact that the last hidden layer carries the highest level of mutual information between the output of hidden layers and the labels [58, 70]. In this regard, and according to the CMI-permutation principle, the stopping criteria encompasses the CMI between the output of the last hidden layer and the labels conditioned on the best genome created in the previous generations (lines #2,7 in Algorithm 3). Moreover, the degradation in the loss (i.e., an increase in the cross-entropy loss) is considered as in the line #4 in Algorithm 3. If the degradation is not observed, the CMI values are compared to ensure that the permuted genomes, i.e., the NNs in generation  $t + 1$ , outperform their respective descendant  $L_{t,*}$ . If not, the algorithm halts and outputs  $L_{T,*} = L_{t,*}$  that is the best genome at the last generation

denoted by  $T$ . Note that no stopping criterion has been previously defined for the NEAT algorithm, as shown in Algorithm 1.

### 5.3 Training and Testing Phases

The training phase of InfoNEAT involves running the algorithm with the fitness function and the genome selection criteria as well as the stopping criteria (based on the fitness and CMI values). The algorithm describing the evolution process within InfoNEAT is discussed in Algorithm 1, the best genome or network selection criteria is discussed in Algorithm 2, and the training stopping criteria is discussed in Algorithm 3.

Neuroevolution techniques such as NEAT evolve the weights and structure of a network from a simple starting point, and usually develop a minimal and a generalizable NN. However, it is challenging for the NEAT to optimize all parts of the network if the learning task concerns multi-class classification [42]. To tackle this, InfoNEAT uses the One-vs-All (OvA) classification technique to develop  $m$  sub-models corresponding to the number of labels or classes (i.e., 256 sub-keys). In other words, this technique turns a multi-class classification problem into a collection of  $m$  binary classification tasks. The sub-models are then combined through *stacking*; that is, an ensemble machine learning technique that combines predictions from multiple classification models via a meta-learner or meta-classifier. In the context of neuroevolution, ensemble approaches have been employed, where the most relevant method to ours is [42] that proposes applying naive Bayes technique. Compared to this, our stacked meta-model learns how to best combine the predictions from multiple well-trained NNs using logistic regression, which has proven more effective than naive Bayes [47].

Moreover, we perform the **k-fold cross-validation**<sup>2</sup> to ultimately create  $k$  different stacked models, which are then all used to provide a combined prediction to the unseen data. For this purpose, we first divide the entire training dataset into  $k$  different folds of the dataset. To train the sub-models and the stacked model, we use  $k - 1$  folds as the training dataset and the remaining one fold of the dataset as the testing dataset. Every time we run the algorithm to get a new stacked model, we use different folds of the dataset.

**Training the sub-models:** We train the sub-models based on the different folds of the dataset created for the k-fold cross-validation. For this purpose, we run InfoNEAT algorithm  $m$  times using  $m$  different, respective datasets, see Figure 4. Note that each of these  $m$  different datasets contains  $k$  folds to perform cross-validation. For each label or class, we make sure that the dataset contains an equal number of traces belonging and not belonging to that particular class as required by the OvA method. The labels in these datasets are then modified accordingly using one-hot encoding where the length of each label is  $m$ . If the data belongs to the particular class, only the index corresponding to that class is 1. All the indices in the labels for traces not belonging to the class are set to 0.

**Training the stacked model:** After  $m$  number of sub-models are trained, a stacked model is then trained which basically combines the predictions from all the sub-models and outputs a final prediction as shown in Figure 4. The predictions from each of the sub-models are a set of probabilities indicating whether the data

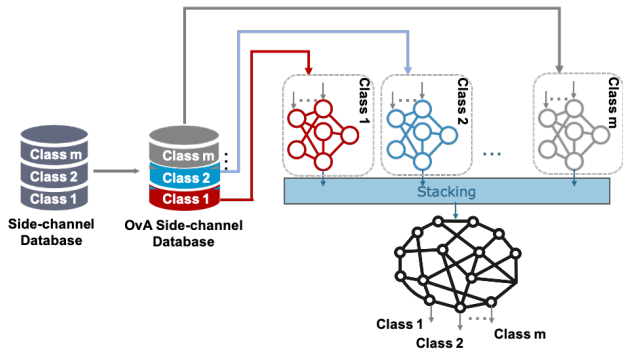


**Figure 4: Schematic of the NEAT algorithm configured to deliver a stacked model. For each class, a sub-model is trained by feeding batches from One-vs-All (OvA) database.**

belongs to a particular class. The stacked model can also be regarded as a **meta-learner** and to train this meta-learner, we first prepare a training dataset for it. This dataset is prepared by using the predictions from all the sub-models after which the dataset along with its actual output is then used to train our meta-learner which in our case is a simple **logistic regression** model.

**Testing phase:** The steps in training the sub-models and the stacked model are repeated  $k$  times to create  $k$  trained stacked models. These models are used against the test dataset to return  $k$  sets of predictions (or **average ranks** in the case of SCA), combined to get an average prediction (or an average rank) for the test data. Notice that we do not use the common ML metrics to test our model due to the fact that the ML metrics, e.g., the accuracy, do not provide relevant information to the attackers; hence, it is not guaranteed that a model with good performance based on ML metrics necessary performs well in the case of SCA [50]. Concretely, we use the SCA-related metrics, namely the average rank, to test our InfoNEAT stacked model.

### 5.4 Discussion of Practical Implementation

Various practical challenges were encountered and resolved during InfoNEAT’s design and execution. They are itemized and discussed below along with pointers to our results.

**Bias and variance in NNs:** A common problem with stochastic algorithms involved in training the NNs is the high variance in the network similar to the case of SCA [61]. In other words, every time the model is fit to a new data point, the network has different sets of weights and parameters which in turn makes different predictions. To deal with this, the weight initialization method is chosen carefully for InfoNEAT (see Appendix C) and the evolution is further controlled by monitoring the fitness and CMI values. On top of this, stacking is used that has also been shown to produce models with lower bias compared to the sub-models used. Furthermore, after a stacked model is trained, we employ the k-fold cross-validation technique to reduce the variability of the stacked model associated with learning new data points (see Figure 16 in Appendix C showing an example of our sub-models that is neither underfitting nor overfitting).

<sup>2</sup>Note that here  $k$  denotes the number of data folds.



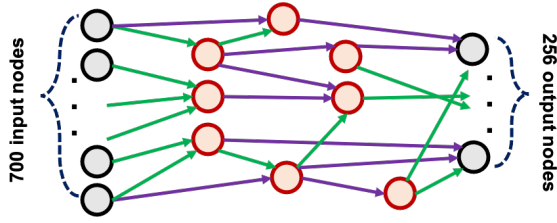


Figure 5: Sample InfoNEAT architecture used for SCA.

**Search space explored by NEAT:** The search space in the case of NNs is the set of all possible weight configurations – the wider and deeper the network is, the larger the search space is. In that sense, the architecture of the network (i.e., the number of layers and number of hidden nodes) can also be considered as part of the search space since they affect the size of the network. Neuroevolution techniques such as NEAT evolve both the weights and NN architecture through crossover and mutation [20]. Thus, compared to traditional optimizers (such as the stochastic gradient descent, SGD) which only optimize the weight, the search space for neuroevolution techniques is considerably larger [1]. In InfoNEAT, this challenge is simplified. InfoNEAT starts the evolution process from small sized network and uses the evolutionary operators, namely the mutation and crossover operators, to explore the search space. But unlike NEAT, InfoNEAT uses the CMI values rather than just the fitness values to help guide evolution. This also helps to achieve an optimally sized network as the hidden nodes are only added if the CMI values do not decrease monotonically.

**Evaluation of multiple *distinct* networks:** A salient feature of NEAT that makes it preferable over other network optimization methods is that NEAT evaluates a population of different networks all at the same time. However, this is only true if the networks are inherently distinct. One of the NEAT methods that help maintain diversity among networks is *speciation*. Speciation has been typically effective for penalizing similar networks by looking at the fitness and the structure of the network. The speciation parameters thus have to be tuned very carefully because of the associated time complexity of evaluating a typical SCA network and converging towards a solution. We discuss some of these parameters in more detail in Section 7.1.1, namely the *compatibility threshold* parameter which helps divide a population of genomes into different species where the genomes between two species are inherently distinct.

**Automatic evaluation of CMI for analyzing and finding the best genome every generation and implementing the stopping criteria:** The methods proposed in the literature calculate CMI for typical CNN and MLPs [67, 68]. However, the network evolved using NEAT is an unusual network as nodes from multiple layers can have a direct connection to each other (not the case for a typical MLP network) as shown in Figure 5. We have addressed this by calculating the CMI for each node based on all of its connections.

## 6 INTRINSIC DIMENSIONALITY

This section includes relevant information to justify why compact NNs, specifically NNs in the context of InfoNEAT, can learn and disclose the sub-keys in SCA. Similar to other applications of NNs, this is thanks to their considerably small difference between training

and test performance. Traditionally, this property was attributed to characteristics of the model family or to the regularization techniques employed during the training process. Recently, it has been demonstrated that a NN can generalize well if the number of parameters goes beyond the number of data points, which usually holds in practice [70]. By analyzing this more thoroughly, the ID has been used to explain properties of NNs, especially the generalizability of the network cf. [3]. Moreover, the training and testing errors are linked to the ID through the bounds as a function of the ID and the total number of parameters in an NN (the number of weights and biases) [45]. In this respect, for a given training or testing error and ID, it is possible to compute the maximum number of parameters. According to the analysis given in [45], if the ID reduces, the number of parameters, and consequently, the size of the NN decrease exponentially. Therefore, in the following paragraphs, we attempt first to re-introduce a method to *estimate* the ID of a dataset containing side-channel traces. We further give an example of the ID estimation for a dataset as a proof of concept.

**ID estimation:** Since for a finite set of points, it is not possible to thoroughly compute the ID, a wide range of estimation techniques have been proposed for this purpose (see, e.g., [11] for a comprehensive survey). In general, the ID can be estimated either globally for the whole data distribution or locally in different regions of the data space. Even for datasets with no ID variations, it is nontrivial to make a connection between global and local ID estimation cf. [4]. On the other hand, for applications like SCA, global ID estimation is challenging due to the lack of representative data points. This can also impair the effectiveness of local ID estimators; hence, recent studies have been dedicated to introducing novel local ID estimators. In particular, when the dataset exhibits a large ID, it can be exponentially hard (as a function of the ID) to sample the local distribution due to the so-called curse of dimensionality [16]. To tackle this, a family of local ID estimators applies the notions belonging to the geometric (or fractal) methods, see, e.g., [16]. For instance, one can refer to CorrDim, DANCo, and FCI estimators discussed in Section 3.3.2. These techniques cover the spectrum of various types of datasets, namely datasets with a small or large ID and ones including noisy samples. This is important to our framework since the ID of the dataset composed of side-channel traces is not a known priori. Moreover, the noise in such a dataset is an even more pressing issue.

Here we give an example of applying these techniques against the ASCAD dataset that serves as a benchmark dataset for SCA (see Section 3.2.1). In doing so, 10,000 traces randomly selected from all the classes in the ASCAD dataset are fed to CorrDim, DANCo, and FCI estimators that are implemented in Matlab [30]. Note that the sub-set of traces chosen for this purpose is balanced, i.e., the number of traces for the classes is (almost) the same. Each experiment is repeated 10 times to examine if the results are consistent. The results obtained through these analyses are depicted in Figure 6. The x-axis shows the 256 classes (i.e., sub-keys) in the dataset, whereas on the y-axis the estimated ID is shown. As expected, the DANCo algorithm yields the results that vary drastically over the repetitions; hence the average of the estimated ID is reported (for more detailed results, see Appendix A). On the contrary, CorrDim and FCI algorithms deliver the same results (with less variation)

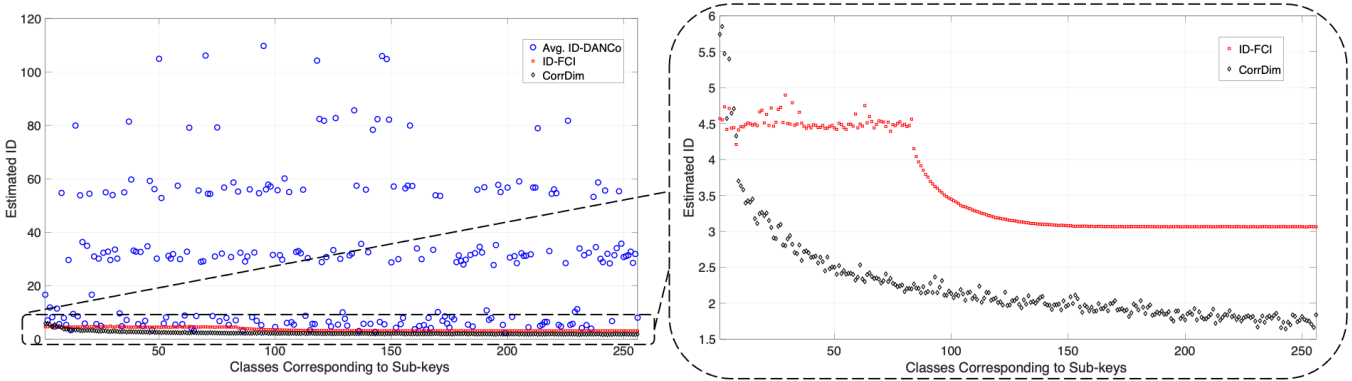


**Figure 6: Intrinsic dimensionality (ID) estimation using DANCo, FCI estimator, and CorrDim. The experiments are repeated 10 times, for which the FCI and CorrDim estimators yield the same results; however, the results of DANCo method show a high level of variation. Hence, for DANCo, the average estimated ID is reported (more results are presented in Appendix A).**

over the repetitions. For each class (i.e., sub-key), the results of applying these methods are comparable, although estimated ID achieved through FCI is more reliable since it is less sensitive to the number of traces and the noise, as discussed before. This analysis implies that NNs with a small number of NN parameters (i.e., compact architectures) can be trained and generalize well to recover the sub-key [45]. In particular, for a given function approximated by the ReLU-equipped NN (i.e., the mapping between the traces and their respective sub-key), the number of parameters in the NN is upper bounded as  $O(\varepsilon^{-1/d})$ , where  $\varepsilon \leq 1$  is the approximation error. In this case, the generalization error is also bounded by  $O(n^{-1/d})$ , cf. [45].

## 7 RESULTS

This section discusses our experimental setup used to train and test the model using InfoNEAT. Results presented here demonstrate the effectiveness of our CMI-based criteria, and in general, InfoNEAT in terms of key recovery.

### 7.1 Experimental Setup

The experiments in this section are conducted on the three different ASCAD databases – ASCADsync, ASCADdesync50, and ASCADdesync100 – as introduced in Section 3.2.1. Moreover, the ASCADsync dataset is **shuffled** to improve the learning process by avoiding any visible or invisible bias induced during the data collection phase. This step has been considered optional in the SCA-related literature [5], although from ML point of view, it is helpful to incorporate into the learning process. All the experiments are run without pre-processing the ASCAD datasets on a high-computing cluster with a total of 8 CPUs allocated per task and a total memory of 80 GB. The CPUs are the Skylake Dell C6420 model with Xeon Gold 6142 processors.

**Number of traces involved in cross-validation, training, and testing:** Figure 7 provides a brief overview of the number of traces used in each of the training and testing phase of the experiment. Note that the SCA-dataset is not balanced meaning that the frequencies of data corresponding to each label are not equal. To address the imbalance in the dataset, we create new balanced datasets based

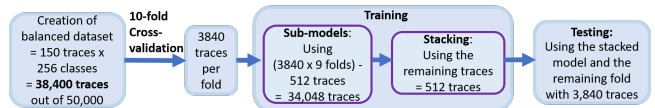


**Figure 7: Overview of the training and testing procedure showing the number of traces involved in each step.**

on all three ASCAD datasets by performing a data-level method, namely the random undersampling [50]. This means that only the maximum possible number of data equally for each class is used. We found this number to be 150, i.e., 150 traces per class are used to create new balanced datasets as shown in Figure 7. Interestingly, InfoNEAT is able to recover the sub-key even when the number of traces per sub-key is reduced (see Section 7.5). After dealing with the imbalance in the dataset, we perform the *10-fold cross-validation* (see Section 5.3), where nine folds of the dataset are used for training the ensembles of sub-models and the stacked model (two traces per class for the stacked model while the rest is used for the sub-models), and the remaining fold of the dataset is used for testing the stacked model. By performing 10-fold cross validation, the performance of InfoNEAT is evaluated using one of the most popular SCA metrics – *average rank* (see Section 3.2).

**7.1.1 Network and configuration parameters.** A typical NEAT architecture is different from a traditional MLP neural network. The main difference as highlighted in Section 4 is that although NEAT networks (as used in InfoNEAT) are feed-forward neural networks, nodes in a specific layer can have multiple direct connections to nodes from different layers as shown in Figure 5. In other words, nodes in the first hidden layer can have direct connection with nodes in second and fourth hidden layers (as highlighted in purple in Figure 5). As discussed in Section 4, the resultant NNs evolved using NEAT are usually quite small (in terms of the number of layers and nodes), yet still quite effective depending on the problem at hand. However, there are several parameters, especially ML-related ones, that need to be decided before the start of the training process for a successful SCA. We summarize them along with their values for InfoNEAT in Table 1.

**Table 1: InfoNEAT parameters set at the start of evolution.**

Parameters	Description	Values
fitness threshold ( $f_t$ )	When the fitness value meets or exceeds this value, the algorithm halts.	0.0
<b>Network parameters</b>		
initial num_hidden ( $n_h$ )	Refers to the initial number of hidden nodes in the network.	10
Activation function	Part of every node and helps calculate the output of the node when given an input or a set of inputs.	Leaky ReLU
Fitness function	Guides the evolution process within the NEAT framework.	Log loss
Number of generations ( $T$ )	Refers to the maximum number of generations the algorithm runs until the fitness criteria is not met. Usually, the algorithm converges before it reaches $T$ generations.	30
Connection add probability ( $P_c$ )	The probability that mutation will add a connection between existing nodes.	0.8
Node add probability ( $P_n$ )	The probability that mutation will add a new node, essentially replacing an existing connection with a node.	1.0
<b>Parameters related to evaluation of multiple distinct networks</b>		
Population size ( $N$ )	Number of genomes or networks considered in a generation.	16
Compatibility threshold ( $t_c$ )	Individuals whose genomic distance is less than this threshold are considered to be part of the same species.	1.8
<b>Initialization of weights and biases - using Xavier technique</b>		
Weights and biases {min, max, init_mean, init_variation}	Weights and biases beyond {min, max} range are clamped. <i>Init_mean</i> and <i>init_variation</i> refer to the distribution of the weights during the start of the algorithm.	{-6.18, 6.18, 0, 1}
Batch size	Size of the training data that is provided to the InfoNEAT algorithm during the evolution process.	150

**Parameters related to evaluation of multiple distinct networks:** The parameter *population size* can be set based on how many networks the user wants to evaluate in parallel. Since most of the experiments were conducted on a 16-core machine, we set this parameter as 16 to efficiently evaluate multiple networks. The parameter *compatibility threshold* is a NEAT parameter that helps maintain diversity in a population of genomes or NNs by comparing the genomic distance of the network with this parameter value. Genomic distance is essentially measured as a linear combination of the number of excess and disjoint genes or nodes, as well as the average weight differences of matching genes or nodes between two genomes or networks [60]. The parameters *connection add probability* and *node add probability* help evolve the size of the network, and are set to high values for this purpose. Furthermore, CMI helps control the size of the network and stops the training at the right time as discussed in Section 7.1.2.

The other parameters mentioned in Table 1 are not as critical; however, our empirical analysis shows that they can influence convergence time as well as the diversity of the neural networks being evaluated in each generation. To set these parameters, we employ commonly used methods as described in Appendix C.

**7.1.2 Incorporation of CMI-based Criteria.** These criteria, as discussed in Section 5.2, can be helpful to select the best genome and stop the training process at the correct time (see Algorithms 2-3). Figure 8 shows the progression of both the fitness and CMI values for the best genome (or network) during each generation for a randomly chosen class. In most cases, log loss is a good criteria to select the best genome, but whenever the fitness values are comparable then we analyze the CMI values as explained in Algorithm 2. We also employ the CMI-based criteria to stop the evolution process at the right time as described in Algorithm 3. Whenever the CMI value and log loss both start to degrade, then we select the best genome from the previous generation as our ultimate model for the class. As shown in Figure 8, we select our ultimate model from generation 6 rather than generation 7 or 8.

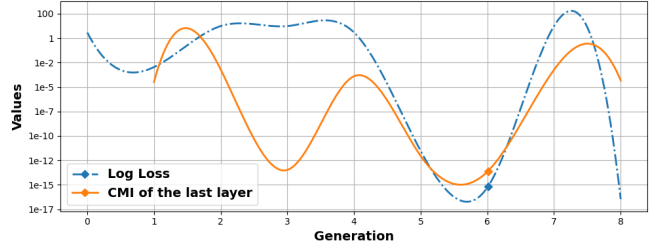


**Figure 8: Log loss and CMI-based criteria values for the last layer versus different generation. These values are obtained for the best genome at each generation. For better readability, the results for one randomly selected class is presented.**

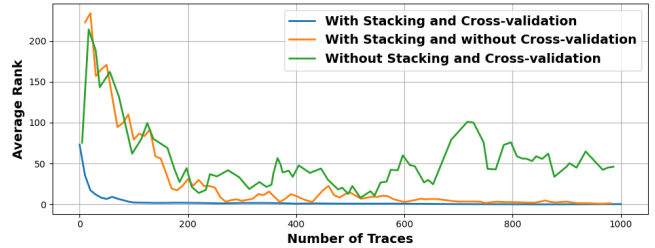


**Figure 9: Comparison of average rank obtained for different models obtained with and without stacking and cross-validation.**

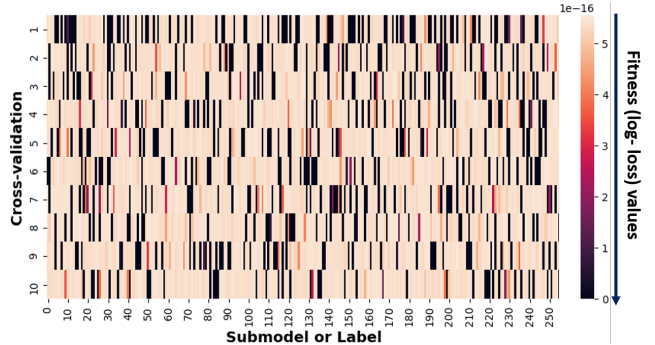


**Figure 10: Heatmap of log loss values for all the 256 submodels trained on the ASCADsync dataset. Darker regions indicate better log loss values.**

## 7.2 Training an Effective Stacked Model

After the configuration parameters are set and the weights and biases appropriately initialized, we now enter the *training phase*. As discussed in Section 7.1, we train 256 different sub-models for the 256 classes using the balanced ASCAD databases and by employing the OvA technique. As shown in Figure 9, with stacking and cross-validation involved, the test metric (average rank in our experiments) improves drastically compared to without stacking and cross-validation. Furthermore, the results of the fitness values of all the 256 sub-models for all ten-folds of the cross-validation are shown in the heatmap plotted in Figure 10. The darker the heatmap region is, the better the fitness value is. Although there are a lot of lightly colored regions in the heatmap, note that the fitness values are in the range of  $10^{-16}$ . This shows that the training of the sub-models is performed extremely well.

**Table 2: Comparison of the time taken for InfoNEAT versus NEAT to train a specific sub-model for each ASCAD dataset.**

ASCAD dataset	With InfoNEAT		With NEAT	
	Average no. of generations	Average generation time [s]	Average no. of generations	Average generation time [s]
Sync	8	67.384	17	91.426
Desync50	9	69.805	19	103.754
Desync100	11	68.361	20	120.682

### 7.3 Time-complexity for InfoNEAT Training

All the steps mentioned in Section 7.1, such as the configuration of NEAT parameters, initialization of weights and batch size, and the inclusion of CMI-based criteria are part of the InfoNEAT algorithm, and they highly contribute to the improvement of the time-complexity associated with training an effective SCA model for different ASCAD datasets. Table 2 summarizes the average time involved in training a particular sub-model using the InfoNEAT algorithm (column labeled as “With InfoNEAT”) and compares this time to the average time taken while using the default NEAT without the CMI-based criteria (column labeled as “With NEAT”). For the default NEAT, we select the batch size of 200 as recommended in [5]. Note that we still employ the OvA classification technique to train the sub-model when using the default NEAT parameters without the CMI-based criteria.

### 7.4 Computation of Average Rank

The trained InfoNEAT models are evaluated against the test or attack dataset based on the average rank, computed by using the rank function provided in the ASCAD package [5]. Figure 11 show the results of using InfoNEAT model against different ASCAD datasets. The results show the effectiveness of InfoNEAT model. As can be seen, InfoNEAT is capable of learning different datasets when trained and tested on the same dataset. More interestingly, the average rank computed by using the model trained on synchronized data to attack or test the desynchronized data is comparable to the other average ranks (trained and tested on the same type of dataset). This shows that the models trained using InfoNEAT are *generalizable* in the sense that they are not sensitive to desynchronization/jittering.

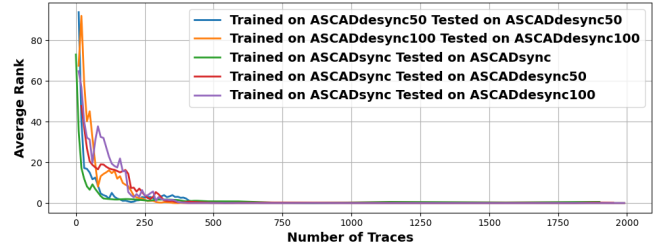
### 7.5 Comparison to State-of-the-Art

Figure 12 shows the comparison of four different networks and InfoNEAT for the ASCADsync dataset. These four different networks are the state-of-the-art MLP networks used for the purpose of SCA, namely the ASCAD network [5], the Ensemble of networks designed in [49], the network designed by Weissbart et al. [63], and the network designed using Bayesian optimization in “I Choose YOU” [65]. As the figure shows, InfoNEAT’s performance is comparable and sometimes even better than some networks such as Weissbart et al. [63] and [65]. We also compare the hyperparameters and the training mechanism of InfoNEAT with the state-of-the-art MLP networks in Table 3. The table shows that the model trained using InfoNEAT is small (only 2 hidden layers), compact (average of 15 nodes in each hidden layer), and requires fewer epochs (on average 8) to train an efficient NN. More precisely, when compared to the most relevant approach [65], InfoNEAT reduces the number

**Table 3: Comparison of the size and training mechanisms of various state-of-the-art MLP networks with InfoNEAT.**

MLP Network	No. of hidden layers	Average No. of nodes in each layer	No. of epochs	No. of training traces	Hyperparameter tuning
ASCAD [5]	6	200	400	40,000	Trial and error
Ensemble [49]	[2,8]*	[100, 1000]*	-	50,000	Randomly selected
Weissbart et al. [63]	6	300	200	20,000	Trial and error
I Choose You [65]	[2,10]*	[100, 400]*	10	50,000	Bayesian optimization and Random Forest
InfoNEAT	2	15	8	38,400	Automatic Neuroevolution

\* This specifies the range of the values that was used to find an optimal value.



**Figure 11: Average rank versus the number of traces across stacked models.**

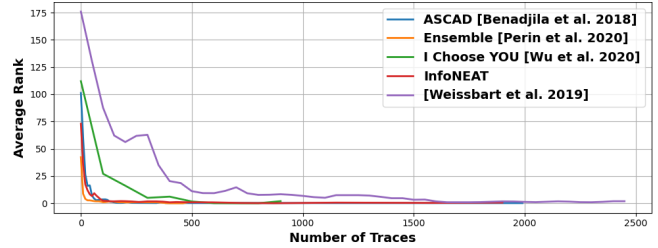


**Figure 12: Performance comparison between various state-of-the-art MLP networks for SCA and InfoNEAT.**

of epochs and nodes in layers by factors of at least 1.25 and 6.6, respectively. Note that for InfoNEAT and for the sake of comparison, we only consider the size of the sub-models because we train them one-by-one, and hence, the size of the stacked model is irrelevant. Moreover, the process of tuning the hyperparameters is completely automatic since InfoNEAT uses evolutionary algorithms to train NNs.

## 8 CONCLUSION

In this paper, we introduce a first of its kind, information theory-based automatic neuroevolution technique that successfully profiles the SCA traces of 256 different classes. This is achieved through use of the CMI-heuristic, NEAT algorithm, OvA decomposition technique, and consequent stacking ensemble learning to train an effective SCA model which is simple, compact, and yet deep enough to successfully extract the sub-key using less than a hundred traces. In addition, we provide a detailed study (and to the best of our knowledge, the first study) on the impact of Intrinsic Dimensionality (ID) of the SCA dataset and prove that the small and compact networks created using InfoNEAT are quite effective in conducting a successful sub-key extraction.



## REFERENCES

- [1] Ahmed Aly, David Weikersdorfer, and Claire Delaunay. 2019. Optimizing Deep Neural Networks with Multiple Search Neuroevolution. *arXiv preprint arXiv:1901.05988* (2019).
- [2] Rana Ali Amjad and Bernhard C Geiger. 2019. Learning Representations for Neural Network-Based Classification Using the Information Bottleneck Principle. *Trans. on Pattern Analysis and Machine Intelligence* 42, 9 (2019), 2225–2239.
- [3] Alessio Ansuini, Alessandro Laio, Jakob H Macke, and Davide Zoccolan. 2019. Intrinsic dimension of data representations in deep neural networks. *arXiv preprint arXiv:1905.12784* (2019).
- [4] Jonathan Bac and Andrei Zinovyev. 2020. Local intrinsic dimensionality estimators based on concentration of measure. In *Intrnl. Joint Conf. on Neural Networks (IJCNN)*. IEEE, 1–8.
- [5] Ryad Benadjila, Emmanuel Prouff, Rémi Strullu, Eleonora Cagli, and Cécile Dumas. 2018. Study of Deep Learning Techniques for Side-Channel Analysis and Introduction to ASCAD database. *IACR Cryptol. ePrint Arch.*, 2018/053 (2018).
- [6] Shivam Bhasin, Anupam Chattopadhyay, Annelie Heuser, Dirmanto Jap, Stjepan Picek, and Ritu Ranjan. 2020. Mind the Portability: A Warriors Guide through Realistic Profiled Side-channel Analysis. In *NDSS 2020*.
- [7] Rajendra Bhatia. 2006. Infinitely Divisible Matrices. *The American Mathematical Monthly* 113, 3 (2006), 221–235.
- [8] Olivier Bronchain, Julien M Hendrickx, Clément Massart, Alex Olshevsky, and François-Xavier Standaert. 2019. Leakage Certification Revisited: Bounding Model Errors in Side-Channel Security Evaluations. In *Annual Intrnl. Cryptol. Conf.* Springer, 713–737.
- [9] Eleonora Cagli, Cécile Dumas, and Emmanuel Prouff. 2015. Enhancing Dimensionality Reduction Methods for Side-Channel Attacks. In *Intrnl. Conf. on Smart Card Research and Advanced Applications*. Springer, 15–33.
- [10] Eleonora Cagli, Cécile Dumas, and Emmanuel Prouff. 2017. Convolutional Neural Networks with Data Augmentation Against Jitter-Based Countermeasures. In *Intrnl. Conf. on Cryptographic Hardware and Embedded Systems*. Springer, 45–68.
- [11] P Campadelli, E Casiraghi, C Ceruti, and A Rozza. 2015. Intrinsic Dimension Estimation: Relevant Techniques and a Benchmark Framework. *Mathematical Problems in Engineering* (2015).
- [12] Kevin M Carter, Raviv Raich, and Alfred O Hero III. 2009. On Local Intrinsic Dimension Estimation and Its Applications. *Trans. on Signal Processing* 58, 2 (2009), 650–663.
- [13] Claudio Ceruti, Simone Bassis, Alessandro Rozza, Gabriele Lombardi, Elena Casiraghi, and Paola Campadelli. 2014. DANco: An intrinsic dimensionality estimator exploiting angle and norm concentration. *Pattern Recognition* 47, 8 (2014), 2569–2581.
- [14] Suresh Chari, Josyula R Rao, and Pankaj Rohatgi. 2002. Template Attacks. In *Intrnl. Workshop on Cryptographic Hardware and Embedded Systems*. Springer, 13–28.
- [15] Julien Doget, Emmanuel Prouff, Matthieu Rivain, and François-Xavier Standaert. 2011. Univariate side channel attacks and leakage modeling. *Journal of Cryptographic Engineering* 1, 2 (2011), 123.
- [16] Vittorio Erba, Marco Gherardi, and Pietro Rotondo. 2019. Intrinsic dimension estimation for locally undersampled data. *Scientific reports* 9, 1 (2019), 1–9.
- [17] European Commission. 2020. The Framework Programme for Research and Innovation. [Online] <https://ec.europa.eu/programmes/horizon2020/en> [Accessed: Jan.15, 2021]. (2020).
- [18] François Fleuret. 2004. Fast Binary Feature Selection with Conditional Mutual Information. *Journal of Machine Learning Research* 5, 9 (2004).
- [19] Damien François, Fabrice Rossi, Vincent Wertz, and Michel Verleysen. 2007. Resampling methods for parameter-free and robust feature selection with mutual information. *Neurocomputing* 70, 7–9 (2007), 1276–1288.
- [20] Edgar Galván and Peter Mooney. 2021. Neuroevolution in Deep Neural Networks: Current Trends and Future Challenges. *Trans. on Artificial Intelligence* (2021).
- [21] Richard Gilmore, Neil Hanley, and Maire O’Neill. 2015. Neural network based attack on a masked implementation of AES. In *Intrnl. Symposium on Hardware Oriented Security and Trust (HOST)*. IEEE, 106–111.
- [22] Luis Gonzalo Sanchez Giraldo, Murali Rao, and Jose C Principe. 2014. Measures of Entropy From Data Using Infinitely Divisible Kernels. *Trans. on Information Theory* 61, 1 (2014), 535–548.
- [23] Phillip Good. 2013. *Permutation Tests: A Practical Guide to Resampling Methods for Testing Hypotheses*. Springer Science & Business Media.
- [24] Alexander Hagg, Maximilian Mensing, and Alexander Asteroth. 2017. Evolving Parsimonious Networks by Mixing Activation Functions. In *Proceedings of the Genetic and Evolutionary Computation Conf.* 425–432.
- [25] Soufiane Hayou, Arnaud Doucet, and Judith Rousseau. 2019. On the Impact of the Activation Function on Deep Neural Networks Training. In *Intrnl. Conf. on Machine Learning*. PMLR, 2672–2680.
- [26] Benjamin Hettwer, Stefan Gehrer, and Tim Güneysu. 2020. Applications of machine learning techniques in side-channel attacks: a survey. *Journal of Cryptographic Engineering* 10, 2 (2020), 135–162.
- [27] Annelie Heuser and Michael Zohner. 2012. Intelligent Machine Homicide. In *Intrnl. Workshop on Constructive Side-Channel Analysis and Secure Design*. Springer, 249–264.
- [28] Anh-Tuan Hoang, Neil Hanley, and Maire O’Neill. 2020. Plaintext: A Missing Feature for Enhancing the Power of Deep Learning in Side-Channel Analysis? *IACR Trans. on Cryptographic Hardware and Embedded Systems* (2020), 49–85.
- [29] Gabriel Hospodar, Benedikt Gierlichs, Elke De Mulder, Ingrid Verbauwhe, and Joos Vandewalle. 2011. Machine learning in side-channel analysis: a first study. *Journal of Cryptographic Engineering* 1, 4 (2011), 293.
- [30] The MathWorks Inc. 2020. version 9.8.0.1417392 (R2020a). [Online] <https://www.mathworks.com/products/matlab.html> [Accessed: Jan.15, 2021]. (2020).
- [31] Nitish Shirish Keskar, Dheevatsa Mudigere, Jorge Nocedal, Mikhail Smelyanskiy, and Ping Tak Peter Tang. 2016. On Large-Batch Training for Deep Learning: Generalization Gap and Sharp Minima. *arXiv preprint arXiv:1609.04836* (2016).
- [32] Jaehun Kim, Stjepan Picek, Annelie Heuser, Shivam Bhasin, and Alan Hanjalic. 2019. Make Some Noise. Unleashing the Power of Convolutional Neural Networks for Profiled Side-channel Analysis. *IACR Trans. on Cryptographic Hardware and Embedded Systems* (2019), 148–179.
- [33] Michael Kirby. 2001. *Geometric Data Analysis: An Empirical Approach to Dimensionality Reduction and the Study of Patterns*. Wiley New York.
- [34] Siddharth Krishna Kumar. 2017. On weight initialization in deep neural networks. *arXiv preprint arXiv:1704.08863* (2017).
- [35] Liran Lerman, Gianluca Bontempi, and Olivier Markowitch. 2015. A machine learning approach against a masked AES. *Journal of Cryptographic Engineering* 5, 2 (2015), 123–139.
- [36] Liran Lerman, Romain Poussier, Gianluca Bontempi, Olivier Markowitch, and François-Xavier Standaert. 2015. Template Attacks vs. Machine Learning Revisited (and the Curse of Dimensionality in Side-Channel Analysis). In *Intrnl. Workshop on Constructive Side-Channel Analysis and Secure Design*. Springer, 20–33.
- [37] Elizaveta Levina and Peter J Bickel. 2005. Maximum Likelihood Estimation of Intrinsic Dimension. In *Advances in neural information processing systems*. 777–784.
- [38] Gabriele Lombardi. 2013. Intrinsic dimensionality estimation techniques. [Online] <https://www.mathworks.com/matlabcentral/fileexchange/40112-intrinsic-dimensionality-estimation-techniques> [Accessed: Apr.20, 2021]. (2013).
- [39] Houssein Maghrebi, Thibault Portigliatti, and Emmanuel Prouff. 2016. Breaking Cryptographic Implementations Using Deep Learning Techniques. In *Intrnl. Conf. on Security, Privacy, and Applied Cryptography Engineering*. Springer, 3–26.
- [40] Zdenek Martinasek, Jan Hajny, and Lukas Malina. 2013. Optimization of Power Analysis Using Neural Network. In *Intrnl. Conf. on Smart Card Research and Advanced Applications*. Springer, 94–107.
- [41] Loïc Masure, Cécile Dumas, and Emmanuel Prouff. 2020. A Comprehensive Study of Deep Learning for Side-Channel Analysis. *IACR Trans. on Cryptographic Hardware and Embedded Systems* (2020), 348–375.
- [42] Tyler McDonnell, Sari Andoni, Elmira Bonab, Sheila Cheng, Jun-Hwan Choi, Jimmie Goode, Keith Moore, Gavin Sellers, and Jacob Schrum. 2018. Divide and Conquer: Neuroevolution for Multiclass Classification. In *Proceedings of the Genetic and Evolutionary Computation Conf.* 474–481.
- [43] Gregory Morse and Kenneth O Stanley. 2016. Simple Evolutionary Optimization Can Rival Stochastic Gradient Descent in Neural Networks. In *Proceedings of the Genetic and Evolutionary Computation Conf.* 2016. 477–484.
- [44] Kevin P Murphy. 2012. *Machine Learning: A Probabilistic Perspective*. MIT press.
- [45] Ryumei Nakada and Masaaki Imaizumi. 2020. Adaptive Approximation and Generalization of Deep Neural Network with Intrinsic Dimensionality. *Journal of Machine Learning Research* 21, 174 (2020), 1–38.
- [46] National Institute of Standards and Technology. 2020. Threshold cryptography project. [Online] <https://csrc.nist.gov/projects/threshold-cryptography> [Accessed: Jan.15, 2021]. (2020).
- [47] Andrew Y Ng and Michael I Jordan. 2002. On Discriminative vs. Generative classifiers: A comparison of logistic regression and naive Bayes. In *Advances in Neural Information Processing Systems*. 841–848.
- [48] Guilherme Perin, Ileana Buhan, and Stjepan Picek. 2020. Learning when to stop: a mutual information approach to fight overfitting in profiled side-channel analysis. *IACR Cryptol. ePrint Arch.* 2020 (2020), 58.
- [49] Guilherme Perin, Łukasz Chmielewski, and Stjepan Picek. 2020. Strength in Numbers: Improving Generalization with Ensembles in Machine Learning-based Profiled Side-channel Analysis. *IACR Trans. on Cryptographic Hardware and Embedded Systems* (2020), 337–364.
- [50] Stjepan Picek, Annelie Heuser, Alan Jovic, Shivam Bhasin, and Francesco Regazzoni. 2019. The Curse of Class Imbalance and Conflicting Metrics with Machine Learning for Side-channel Evaluations. *IACR Trans. on Cryptographic Hardware and Embedded Systems* 2019, 1 (2019), 1–29.
- [51] Stjepan Picek, Annelie Heuser, Guilherme Perin, and Sylvain Guilley. 2019. Profiling Side-channel Analysis in the Efficient Attacker Framework. *IACR Cryptol. ePrint Arch.*, Report 2019/168 (2019).
- [52] Stjepan Picek, Ioannis Petros Samiotis, Jaehun Kim, Annelie Heuser, Shivam Bhasin, and Axel Legay. 2018. On the Performance of Convolutional Neural

- Networks for Side-channel Analysis. In *Intr. Conf. on Security, Privacy, and Applied Cryptography Engineering*. Springer, 157–176.
- [53] Mathieu Renaud, François-Xavier Standaert, Nicolas Veyrat-Charvillon, Dina Kamel, and Denis Flandre. 2011. A Formal Study of Power Variability Issues and Side-Channel Attacks for Nanoscale Devices. In *Annual Intr. Conf. on the Theory and Applications of Cryptographic Techniques*. Springer, 109–128.
- [54] Jorai Rijsdijk, Lichao Wu, Guilherme Perin, and Stjepan Picek. 2021. Reinforcement Learning for Hyperparameter Tuning in Deep Learning-based Side-channel Analysis. *Cryptol. ePrint Arch., Report 2021/071* (2021).
- [55] Andrew M Saxe, Yamini Bansal, Joel Dapello, Madhu Advani, Artemy Kolchinsky, Brendan D Tracey, and David D Cox. 2019. On the information bottleneck theory of deep learning. *Journal of Statistical Mechanics: Theory and Experiment* 2019, 12 (2019), 124020.
- [56] Werner Schindler, Kerstin Lemke, and Christof Paar. 2005. A Stochastic Model for Differential Side Channel Cryptanalysis. In *Intr. Workshop on Cryptographic Hardware and Embedded Systems*. Springer, 30–46.
- [57] Jacob Schrum and Risto Miikkulainen. 2015. Discovering Multimodal Behavior in Ms. Pac-Man Through Evolution of Modular Neural Networks. *Trans. on Computational Intelligence and AI in Games* 8, 1 (2015), 67–81.
- [58] Ravid Shwartz-Ziv and Naftali Tishby. 2017. Opening the Black Box of Deep Neural Networks via Information. *arXiv preprint arXiv:1703.00810* (2017).
- [59] François-Xavier Standaert, Tal G Malkin, and Moti Yung. 2009. A Unified Framework for the Analysis of Side-Channel Key Recovery Attacks. In *Annual Intr. Conf. on the Theory and Applications of Cryptographic Techniques*. Springer, 443–461.
- [60] Kenneth O Stanley and Risto Miikkulainen. 2002. Evolving Neural Networks through Augmenting Topologies. *Evolutionary Computation* 10, 2 (2002), 99–127.
- [61] Daan van der Valk and Stjepan Picek. 2019. Bias-variance Decomposition in Machine Learning-based Side-channel Analysis. *IACR Cryptol. ePrint Arch.* 2019 (2019), 570.
- [62] Daan van der Valk, Stjepan Picek, and Shivam Bhasin. 2020. Kilroy Was Here: The First Step Towards Explainability of Neural Networks in Profiled Side-Channel Analysis. In *Intr. Workshop on Constructive Side-Channel Analysis and Secure Design*. Springer, 175–199.
- [63] Leo Weissbart, Stjepan Picek, and Lejla Batina. 2019. On the Performance of Multilayer Perceptron in Profiling Side-channel Analysis. *IACR Cryptol. ePrint Arch.* 2019 (2019), 1476.
- [64] Leo Weissbart, Stjepan Picek, and Lejla Batina. 2019. One Trace Is All It Takes: Machine Learning-Based Side-Channel Attack on EdDSA. In *Intr. Conf. on Security, Privacy, and Applied Cryptography Engineering*. Springer, 86–105.
- [65] Lichao Wu, Guilherme Perin, and Stjepan Picek. 2020. I Choose You: Automated Hyperparameter Tuning for Deep Learning-based Side-channel Analysis. *IACR Cryptol. ePrint Arch.* 2020 (2020), 1293.
- [66] Shujian Yu, Luis Gonzalo Sanchez Giraldo, Robert Jenssen, and Jose C Principe. 2019. Multivariate Extension of Matrix-Based Rényi’s  $\alpha$ -Order Entropy Functional. *Trans. on Pattern Analysis and Machine Intelligence* 42, 11 (2019), 2960–2966.
- [67] Shujian Yu and José C Principe. 2019. Simple Stopping Criteria for Information Theoretic Feature Selection. *Entropy* 21, 1 (2019), 99.
- [68] Shujian Yu, Kristoffer Wickstrøm, Robert Jenssen, and José C Principe. 2020. Understanding Convolutional Neural Networks With Information Theory: An Initial Exploration. *Trans. on Neural Networks and Learning Systems* (2020).
- [69] Gabriel Zaid, Lilian Bossuet, Amaury Habrard, and Alexandre Venelli. 2020. Methodology for Efficient CNN Architectures in Profiling Attacks. *IACR Trans. on Cryptographic Hardware and Embedded Systems* 2020, 1 (2020), 1–36.
- [70] Chiyuan Zhang, Samy Bengio, Moritz Hardt, Benjamin Recht, and Oriol Vinyals. 2016. Understanding deep learning requires rethinking generalization. *arXiv preprint arXiv:1611.03530* (2016).
- [71] Yuanyuan Zhou and François-Xavier Standaert. 2019. Deep learning mitigates but does not annihilate the need of aligned traces and a generalized ResNet model for side-channel attacks. *Journal of Cryptographic Engineering* (2019), 1–11.

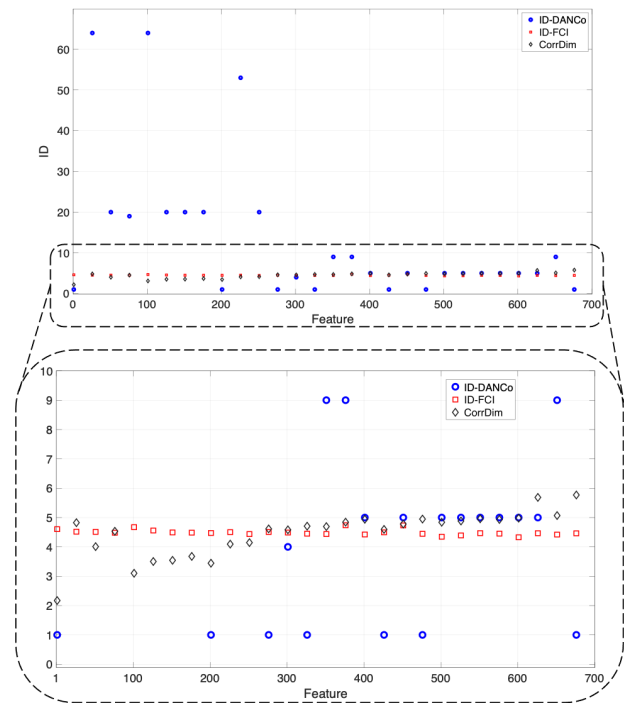
## Appendix A. Related Work at a Glance

Table 4 summarizes some of the most relevant studies discussed in detail in Section 2.

## Appendix B. ID Estimation

This appendix aims to expand on the results obtained for ID estimation. Figure 13 depicts the impact of under-sampling on the ID estimated for one class randomly chosen from the ASCAD dataset. For each of the 10,000 traces, the sub-set  $\{x_1, x_2, \dots, x_k\}$  ( $k \in \{25, 50, 75, \dots, 700\}$ , see x-axis), out of 700 features as in the ASCAD traces, is given to the algorithms to reflect the scenario

of under-sampling. The ID estimation could depend heavily on  $k$  [12] if the estimator is not robust against under-sampling. This is exactly the case for the DANCo algorithm, where the results are highly variable for the sub-sets of the traces. In contrast to this, the results obtained by applying the CorrDim, and especially FCI, are more consistent. This, once again, puts particular emphasis on the importance of choosing an appropriate algorithm, for instance, FCI, for ID estimation.



**Figure 13: ID estimation using DanCo, full correlation integral (FCI) estimator, and the correlation dimension (CorrDim).**

The above analysis focuses on the impact of making changes within one class of the data; however, it is also interesting to examine how robust the estimators are reliable, i.e., yielding the same results when the experiment is repeated. For this purpose, we repeated the experiment described above 10 times for each class. Figure 14 depicts the results of applying the estimators. For the sake of readability, the first 32 classes are shown on the x-axis in Figure 14a, although the same trend is observed for all 256 classes. In particular, for some of the classes (e.g., class 14 as shown in Figure 14a), a significant variation in the results is observed. This does not hold for FCI and CorrDim estimators delivering the same result in the repeated experiments as shown in Figure 14b.

## Appendix C. Network and Configuration Parameters

Here we expand on why and how some of the parameters in NNs are set in the InfoNEAT algorithm, which is tuned to launch key-recovery attacks against side-channel traces.



**Table 4: Table showing the most recent and state-of-the-art works in the field of SCA. The table also elaborates on the problem investigated as well as the comparison to our approach, InfoNEAT. In this table, RF, SVM refer to random forest and support vector machine algorithms, respectively.**

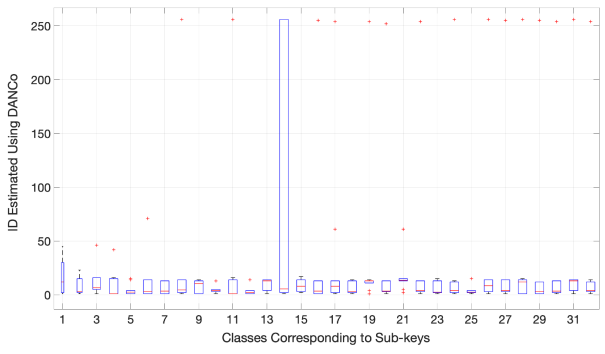
Ref.	Problem investigated	Method	Comparison to our approach (InfoNEAT)
[62]	Explains why MLP works, how the internal nodes are working, and how different they are compared to other models in terms of the internal representation	MLP	This work ends up using a smaller network and smaller training dataset similar to our approach.
[54]	Talks about the problems related to traditional deep learning models- they are complex and there are too many hyperparameters to tune.	CNN	This work uses reinforcement learning (RL) techniques to tune the hyperparameters of CNN.
[28]	Uses the plaintext feature to make the ML models more powerful. Claims that CNN is most successful because of their effectiveness with raw data.	CNN	Without considering the plaintext, our approach along with [49, 62, 63] have been quite effective and comparable to the works using CNN.
[48]	Discusses a stopping criterion based on the analysis of mutual information.	MLP	We use Matrix-based Rényi’s $\alpha$ -entropy conditional mutual information rather than usually applied mutual information to define stopping criterion. Network architecture and other hyperparameters are evolved automatically.
[65]	This work tunes the hyperparameters using Bayesian optimization.	CNN, MLP	Bayesian optimization is used to output a set of hyperparameters, where each set used to train a model. The mechanism to find the best model (i.e., without underfitting or overfitting) is not automatic, in contrast to InfoNEAT. Our approach starts from a minimal size network and gradually evolves the network size and parameters automatically based on cross-entropy loss and CMI-values.
[26]	Surveys the state-of-the-art techniques used for the purpose of SCA. And explains that most of the techniques including CNN and MLP are quite comparable when it comes to SCA.	CNN, MLP	In line with this survey, we use our methodology to train compact MLP-like networks.
[49]	Explains that output class probabilities are sensitive to small changes and thus the developed model is not generalizable. They use ensemble of different models to create a generalizable model.	MLP	We also use ensembles of models (stacking) to develop an effective model. Our stacked model involves submodel for each class, devised using the One-vs-All classification technique. And the whole training process is automated.
[63]	Evaluates the performance of MLP and shows that they are quite effective for the purpose of SCA.	MLP	We also show that MLP-like network is very effective for SCA.
[50]	Discusses the metrics that should be used for evaluating the models developed for the purpose of SCA.	MLP	We use the same metrics especially the average rank to evaluate our InfoNEAT model.
[64]	Shows how all ML techniques are effective in attacking the EddSA, especially CNN which was able to break the implementation with a single measurement.	RF, SVM, CNN	They attack a different dataset compared to us, but nevertheless, show that only few traces are required for an effective SCA.
[52]	Evaluates the performance of CNN and MLP for the purpose of SCA. Also shows that considering the minor performance gains that CNN offers, it is not worthy to invest time and resource to design such a complex network.	CNN, MLP	We therefore use InfoNEAT to design simple and compact MLP-like networks and show that they are quite effective.
[5]	Introduces the ASCAD dataset structured in a similar way as compared to a typical ML dataset.	CNN, MLP	We use the ASCAD dataset to evaluate our model and our results are comparable to the ones presented in this paper.

**Initialization of weights and batch size for training:** To prevent convergence issues, including the *saturation problem* [34], we look at two initialization techniques, namely He and Xavier. Figures 15a and 15b show the results of using the aforementioned initialization techniques in terms of log loss values for models trained and tested with different batch sizes. Note that we select the batch data from the dataset randomly, and we make sure that the data is balanced and unbiased. Moreover, for the sake of readability, we present these results for one class (sub-key), although similar observations are made for other classes. In this case, we use the same batch size for training and testing. Based on our results, the He initialization can lead to underfitting (see the curve in Figure 15a for batch size being greater than 250). Moreover, a sharp minimum is observed when batch size is equal to 100 that can result in poor generalization [31]. Although it can be thought that the Xavier initialization is not a suitable method for networks with ReLU activation function, as our MLPs are not considerably deep, Xavier initialization can be as powerful as He initialization [34]; hence, we choose Xavier initialization.

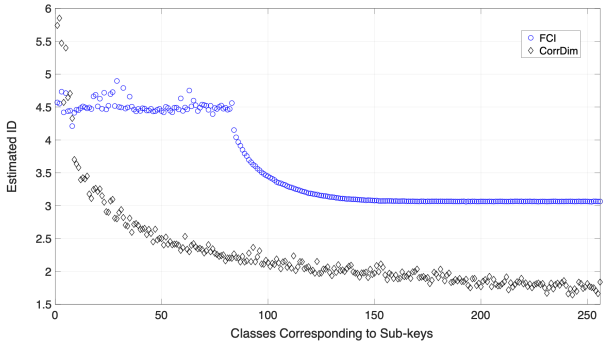
**Batch size selection:** To select the **batch size**, one has to make a trade-off between the size of the batches and the speed of training and generalization error. On the one hand, reducing the size of the batches can have a noise-like effect that is useful for regularizing the data. On the other hand, choosing a larger batch size has been considered as a solution to speed up the training by parallelizing computations. In contrast to this, as reported in [43], EAs can run significantly faster by using smaller batch sizes. Hence, to keep the

generalization gap as small as possible, we focus on the batch sizes 100 and 150. To speed up the training, we measure the average time spend to evolve the genomes before the algorithm halts, which is 653 s and 582 s for batch size equals to 100 and 150, respectively. Therefore, we use the batch size of 150. To observe the impact of this, the diagnostic learning curves are drawn, where the Xavier initialization technique is applied to train the model. The fittest genome or network in each generation is then tested against the test data, and the corresponding log loss values are plotted in Figure 16. The figure shows that the models trained with InfoNEAT are neither overfitting nor underfitting. This is a good sign that the trained model will be generalizable (see Section 7.4 for more detail). Additionally, the selection of Xavier initialization is further justified based on this result.

**The fitness function and the fitness threshold:** One of the major functions that guides the evolution process within the NEAT framework is the objective function or commonly known as the *fitness function*. The fitness function which is specified by the user is used to evaluate the quality of the solution or the genome. In the case of InfoNEAT, we have selected *logistic loss* (hereafter called log loss) as our fitness function as shown in Section 4. This is due to the fact that calculating log loss can give the same quantity as calculating the cross-entropy. Specifically, log loss is one of the most commonly used loss functions which measures the performance of a classification model whose output is a probability value ranging from 0 to 1. The lower the log loss value, the better the model is. With the fitness function selected, we must also specify the



(a)

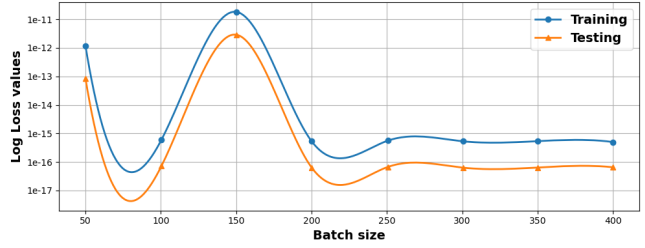


(b)

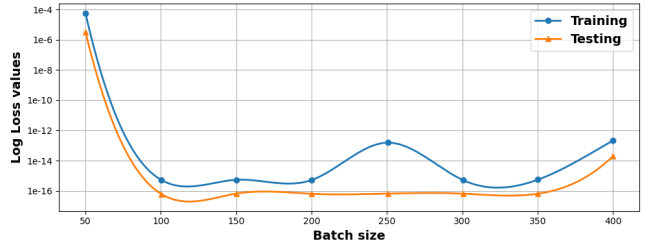
**Figure 14: Estimation of the ID for classes corresponding to the sub-keys. For the sake of readability, the results for the DANCo algorithm are presented for the first 32 classes.**

fitness threshold, the value when it is reached halts the evolutionary algorithm. This threshold value is set as 0 as specified in Table 1.

**Network parameters:** One of the most important network parameters is the activation function. In this paper, we have selected the *Leaky ReLU* or Leaky Rectified Linear Unit as our activation function for all the nodes (except the output nodes) rather than the widely used ReLU activation function (see Table 1). This was done to prevent the well-known "dying ReLU" problem – the scenario when a large number of the nodes output zero because of their inputs being negative, which causes the network to saturate early and train very slowly [25]. Furthermore, Leaky ReLU has been shown to have better performance compared to ReLU and other activation functions such as tanh, sigmoid, etc. [25]. For output nodes, we have selected the *softmax* as our activation function which is one of the commonly used output layer activation function in multi-class classification problems. Softmax assigns probability values to each class or output node such that the sum of these probabilities is 1.



(a)



(b)

**Figure 15: Log loss values for different batch sizes. The weights and biases are initialized based on (a) He, and (b) Xavier initialization techniques. The results are shown for a randomly chosen class.**

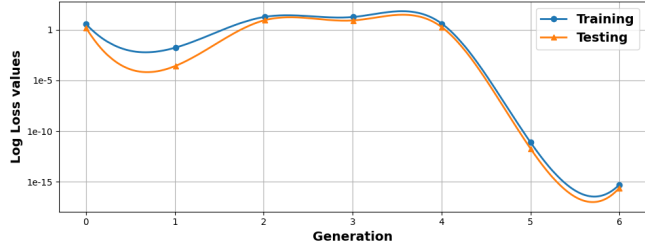


**Figure 16: Learning curve showing the log loss values for different generations. The training and the testing curve values are obtained using the best trained model against the corresponding training and testing dataset in each generation respectively. The result is obtained for a randomly chosen class and the batch size is set to 150.**